The Retinal Crumbs Complex: from animal models and retinal organoids to therapy

Quinn, P.M.J.

Chapter 3

CRB2 in immature photoreceptors determines the superior-inferior symmetry of the developing retina to maintain retinal structure and function

P.M. Quinn, C.H. Alves, J. Klooster and J. Wijnholds

Human Molecular Genetics, 2018, 27, 3137–53.

ABSTRACT

The mammalian apical-basal determinant Crumbs homolog-1 (CRB1) plays a crucial role in retinal structure and function by the maintenance of adherens junctions between photoreceptors and Müller glial cells. Patients with mutations in the *CRB1* gene develop retinal dystrophies, including early-onset retinitis pigmentosa and Leber congenital amaurosis. Previously, we showed that *Crb1* knockout mice developed a slow-progressing retinal phenotype at foci in the inferior retina, although specific ablation of *Crb2* in immature photoreceptors leads to an early-onset phenotype throughout the retina. Here, we conditionally disrupted one or both alleles of *Crb2* in immature photoreceptors, on a genetic background lacking *Crb1*, and studied the retinal dystrophies thereof. Our data showed that disruption of one allele of *Crb2* in immature photoreceptors caused a substantial aggravation of the *Crb1*phenotype in the entire inferior retina. The photoreceptor layer showed early-onset progressive thinning limited to the inferior retina, although the superior retina maintained intact. Surprisingly, disruption of both alleles of *Crb2* in immature photoreceptors further aggravated the phenotype. Throughout the retina, photoreceptor synapses were disrupted and photoreceptor nuclei intermingled with nuclei of the inner nuclear layer. In the superior retina, the ganglion cell layer appeared thicker because of ectopic nuclei of photoreceptors. In conclusion, the data suggest that CRB2 is required to maintain retinal progenitor and photoreceptor cell adhesion and prevent photoreceptor ingression into the immature inner retina. We hypothesize, from these animal models, that decreased levels of CRB2 in immature photoreceptors adjust retinitis pigmentosa because of the loss of CRB1 into Leber congenital amaurosis phenotype.

INTRODUCTION

In humans, the Crumbs homolog-1 (*CRB1*) gene is mutated in a diverse spectrum of retinal dystrophies with variable phenotypes, including autosomal recessive Leber congenital amaurosis (LCA) and retinitis pigmentosa (RP) (1–3). Despite a genetic overlap, these are two clinically distinct inherited retinal dystrophies (4). Variations in the *CRB1* gene account for 7–17% of LCA cases and 3–9% of nonsyndromic autosomal recessive RP cases (5,6). LCA is a group of early-onset retinal dystrophies leading to blindness from near birth typically characterized by abnormal pupillary reflex, nystagmus, and non-recordable or severely attenuated electroretinogram (ERG) responses (7–11). Mutations in the *CRB1* gene cause LCA type 8 which is characterized by a thickening and abnormal layering of the retina not observed in other types of LCA (2,12,13). However, some LCA causing *CRB1* mutations have been associated with an unchanged or thinner retina (14,15). RP is a clinically heterogeneous disorder characterized by night blindness and progressive loss of visual field due to degeneration of rod photoreceptors (4). Mutations in the *CRB1*gene cause RP type 12 which is characterized by a preservation of the para-arteriolar retinal pigment epithelium (PPRPE) and progressive loss of visual field in early childhood due to macular involvement (1,16). However, disease onset in *CRB1*-RP is highly variable with some patients showing symptoms after the first decade of life (7). Other *CRB1*-related clinical features include Coats-like exudative vasculopathy, pigmented paravenous chorioretinal atrophy, macular atrophy, nanophthalmos, keratoconus, and RP without PPRPE (14,17–23). Despite more than 230 pathogenic variants being identified for the *CRB1* gene (see http://exac.broadinstitute.org/transcript/ ENST00000367400 and http://databases.lovd.nl/shared/variants/ CRB1), there is not a clear genotype–phenotype correlation.

In mammals, there are three CRB protein family members, CRB1–3. CRB1 and CRB2 proteins have large extracellular domains comprised of epidermal growth factor-like and laminin-A globular domains, a single transmembrane domain, and a short intracellular domain of 37 amino acids containing a FERM protein binding motif adjacent to a C-terminal PDZ protein binding motif (24). CRB3 shares with CRB1 and CRB2 the short intracellular and single transmembrane domain, but CRB3 lacks the large extracellular domain. The C-terminal amino-acids ERLI in the PDZ domain allows for interaction of the CRB proteins with specific PDZ-binding adaptor proteins, such as PALS1 and PAR6 (25,26). Interaction with PALS1 leads to the assembly of a core CRB complex. PALS1 binds through its N-terminal L27 protein-binding domain to the L27 domain of multiple PDZ-domain proteins MUPP1 or PATJ (27). In the retina, the CRB complex contributes to the maintenance of adherens junctions (AJs) between retinal progenitor cells, Müller glial cells, and rod and cone photoreceptors cells, being crucial for retinal structure and function. The CRB complex is located in the aforementioned cell types at the subapical region (SAR) adjacent to AJs at the outer limiting membrane (OLM) (28–30). The localization of CRB1 and CRB2 at the SAR is the same in Müller glial cells of mice and human (30–34). However, there are

some differences of localization of the CRB proteins in photoreceptors of mouse versus human. Mouse photoreceptors do not express the CRB1 protein, although *Crb1* transcripts are detectable in these cells (30,32,35). Studies performed using human post-mortem retina demonstrated that the CRB1 protein localizes at the SAR of photoreceptors, whereas CRB2 protein localizes at a distance from the SAR in the photoreceptor inner segments (31,34). Some rodent mutant *CRB* models with naturally-occurring or introduced mutations in the *Crb1*gene have been described (3,28–31,36–42). However, these models cannot be used to test the efficacy of photoreceptor-specific gene therapy vectors expressing *CRB2* nor reveal all retinal physiological functions of CRB2 in immature photoreceptors.

Similar to mice lacking CRB1, retinal dystrophy models of other CRB complex members such as CRB2, PALS1 (also called MPP5) and MPP3 showed disruptions of adherence junctions at the OLM (28,39,43–45). Recent studies revealed a mild or severe retinal phenotype in *Crb1* mice dependent on the levels of CRB2 in retinal progenitor cells (29,31). Mice lacking CRB1 show retinal dystrophy at foci in the inferior retina, with protrusion of rows of photoreceptor nuclei into the inner- and outer-segment layer and displacement of photoreceptor nuclei into the photoreceptor synaptic layer. These mice lacking CRB1 mimic a slow progressing RP-like phenotype (30). The loss of mouse CRB2 specifically in retinal radial glial progenitor cells or immature photoreceptors leads to early disruption of the retinal lamination throughout the retina with a severe attenuation of the retinal function. The phenotype of the retinas of these mice mimics an early-onset RP-like phenotype (28,39). The loss of CRB1 and CRB2 in progenitor cells results in a thickening of the retina due to overgrowth of late-born retinal cell types such as photoreceptors, Müller glial cells and bipolar cells (29). Recent work on *CRB* gene therapy suggested the need for CRB proteins in adjacent Müller glial cells and photoreceptors to maintain a functional adult retina (3,34).

Here, to investigate the physiological role(s) of CRB2 in photoreceptors and adjacent retinal progenitor and Müller glial cells, we studied the conditional disruption of one or both alleles of CRB2 in immature photoreceptors on a genetic background lacking *Crb1*. Our data show that reduced levels of CRB2 in immature photoreceptors resulted in a phenotype similar to early-onset RP, although full ablation of *Crb2* from immature photoreceptors produced a phenotype mimicking LCA. The severity of phenotype is significantly increased in retinas lacking CRB1 with reduced levels of CRB2 in immature photoreceptors compared with retinas only lacking CRB1. These double mutant retinas showed extensive lamination defects in the inferior retina, photoreceptor cell death and loss of retinal activity as measured by ERG. Interestingly, retinas with reduced levels of CRB2 in immature photoreceptors showed a most severe phenotype at the inferior side of the retina, whereas complete loss of CRB2 further aggravated the phenotype and showed a most severe phenotype at the superior side of the retina. The retinal dystrophy models showed, therefore, retinal superior/inferior asymmetry of retinal degeneration in the superior versus inferior retina, suggesting an important role for

CRB2 in immature photoreceptors in determining the superior-inferior symmetry of the developing retina to maintain retinal structure and function.

RESULTS

Reduced levels of CRB2 in immature photoreceptors leads to retinal function impairment

Previously, we studied the contribution of CRB2 in retinal progenitors to the CRB1 retinal phenotype, in these studies the *Crb2* gene was ablated in retinal progenitors and therefore also in photoreceptors and Müller glial cells (29,31). To study the contribution of CRB2 in immature photoreceptors to the CRB1 phenotype, we compared the phenotypes of retinas with lowered levels of CRB2 in immature photoreceptors, $Crb1^{KO}Crb2^{Low\text{-}imPRC}$, with loss of CRB2 in immature photoreceptors, $Crb1^{KO}Crb2^{\Delta imPRC}$, and with littermate control mice knockout for CRB1 but with normal levels of CRB2. Schematic models on the presence of CRB1 and CRB2 in progenitor cells, Müller glial cells, rod and cone photoreceptors cells are shown in Supplementary Material, Figure S1.

Both the $Crb1^{KO}Crb2^{\Delta imPRC}$ and $Crb1^{KO}Crb2^{Low\text{-}imPRC}$ mice were fertile, but the $Crb1^{KO}Crb2^{\Delta imPRC}$ mice showed a reduced Mendelian ratio of progeny than expected when analysed at postnatal day (P) 10 (Supplementary Material, Fig. S2A). Previously we reported a high incidence of hydrocephalus in the $Crb2^{\Delta imPRC}$ (39) mice. Here when backcrossed onto 100% C57BL/6JOlaHsd genetic background all $Crb1^{KO}Crb2^{\Delta imPRC}$mice developed severe hydrocephalus. The cause of hydrocephalus is not clear but may be due to leakage of the Cre driver in non-specific areas such as the brain. Hydrocephalous has also been reported in $aPKC\lambda^{flox/flox}$/*Crx-cre* mice (46). In *Yap*-deficient mice the apical integrity of the ventral aqueduct is compromised, showing disruption of the CRB complex and AJs, leading to hydrocephalous (47). This highlights a possible role for CRB proteins in the ependymal cells of the ventral aqueduct. However, it is unlikely to cause or affect the retinal phenotypes we observed. These $Crb1^{KO}Crb2^{\Delta imPRC}$ mice showed severe loss of bodyweight from postnatal day 9 (P9; Supplementary Material, Fig. S2C) and died between the second and third postnatal weeks (Supplementary Material, Fig. S2B and D). Retinal function by electroretinography was not assessed in $Crb1^{KO}Crb2^{\Delta imPRC}$ retina due to reaching a humane endpoint. Therefore, we only analysed the retinal function of the $Crb1^{KO}Crb2^{Low\text{-}imPRC}$ which do not have hydrocephalus.

Mice lacking CRB1 showed disruptions at the OLM but normal retinal function as measured ERG (30). Also, $Crb2^{Low\text{-}imPRC}$ mice with reduced levels of Crb2 showed normal retinal function as measured by ERG but in this case without disruptions at the OLM (39). Here, we performed ERG in 1-, 3- and 6-month-old $Crb1^{KO}Crb2^{Low\text{-}imPRC}$double mutant mice and age-matched control mice (Fig. 1). At 1 month of age, a reduction in scotopic a-wave but not b-wave amplitudes was detectable

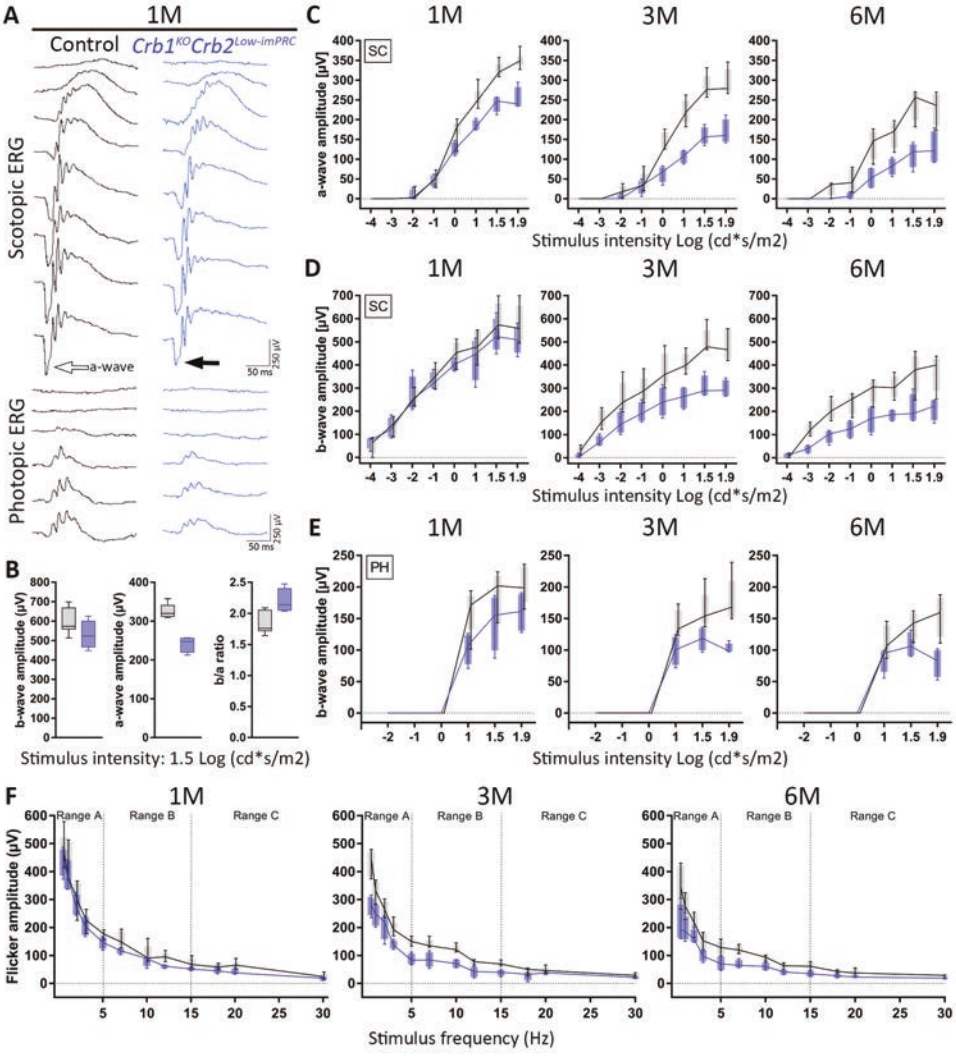

Figure 1. Progressive loss of retinal function in *Crb1^{KO}Crb2$^{Low\text{-}imPRC}$* mice. Electroretinographic analysis of 1-, 3- and 6-month(s)-old control (black) and *Crb1^{KO}Crb2$^{Low\text{-}imPRC}$* affected mice (blue). (A) Scotopic and photopic single-flash intensity series from representative animals at 1 month of age. The control scotopic a-wave is indicated by the open arrow and the black arrow points to the attenuated a-wave of the *Crb1^{KO}Crb2$^{Low\text{-}imPRC}$*. (B) Quantitative evaluation of scotopic single- flash b-wave, a-wave amplitudes (1.5 log cd s/m^2) and the corresponding b-wave/a-wave amplitude ratio (b/a ratio). (C, Dand E) Time course single-flash ERG data from 1- (left), 3- (middle) and 6- (right) month-old mice. Scotopic (SC) a-wave (C) and scotopic and photopic (PH) b-wave amplitudes (D and E, respectively) plotted as a function of the logarithm of the flash intensity. (F) Time course of flicker response amplitudes from 1- (left), 3- (middle) and 6- (right) month-old mice. Boxes indicate the 25 and 75% quantile range and

whiskers indicate the 5 and 95% quantiles, and the intersection of line and error bar indicates the median of the data (box-and-whisker plot). Number of animals used: 1-month old (1M): seven controls and four *Crb1^{KO}Crb2$^{Low\text{-}imPRC}$*; 3M: five controls and four *Crb1^{KO}Crb2$^{Low\text{-}imPRC}$*; 6M: four per group.

(Fig. 1A). Analysis of the b/a ratio showed a higher ratio in *Crb1^{KO}Crb2$^{Low\text{-}imPRC}$* mice than control mice (Fig. 1B). At 3 and 6 months of age, there was further loss of retinal function. Both the scotopic a- and b-wave amplitudes showed significant reductions (Fig. 1C and D). The photopic b-wave amplitudes showed a significant reduction at 3 months of age but only at high stimulus intensity (Fig. 1E). The flicker ERG showed reductions at 3 and 6 months of age in ranges A and B, the rod pathway and the cone ON-pathway, respectively (Fig. 1F). Together the electroretinography data showed that removal of one allele of CRB2 in immature photoreceptors leads to a decrease in photoreceptor function from 1 month of age, suggesting an early-onset and progressive deterioration of the rod and cone systems.

Reduced levels of CRB2 in immature photoreceptors results in a severe inferior retinal phenotype

Morphological analysis of the superior and inferior retina of *Crb1^{KO}Crb2$^{Low\text{-}imPRC}$* mice was carried out from P10 till 6 months of age. The superior part of the control retina (Fig. 2A, D and G) and the *Crb1^{KO}Crb2$^{Low\text{-}imPRC}$* retina (data not shown) was unaffected at 1 month of age. However, morphological alterations of the *Crb1^{KO}Crb2$^{Low\text{-}imPRC}$*superior retina were found adjacent to the optic nerve head (ONH) and extended to the inferior side of the retina from the ONH to the peripheral inferior retina (Supplementary Material, Fig. S3). In 1-month-old *Crb1^{KO}Crb2$^{Low\text{-}imPRC}$* retinas at the superior side close to the ONH (Fig. 2B) and at the inferior side (Fig. 2C), we detected half-rosettes of the outer nuclear layer (ONL). Additionally, we detected, focal protrusions of nuclei from the ONL into the inner- and outer-segment layer. Interestingly, the half-rosettes had an organized OLM and photoreceptor segments (Fig. 2C). The OLM was visible at the superior side in the entire control retina (Fig. 2D) and *Crb1^{KO}Crb2$^{Low\text{-}imPRC}$* retina on histological sections analysed at 1, 3 and 6 months of age (overview stitches 1, 3 and 6 months of age, Supplementary Material, Figs S3 and S4). Although close to the ONH of the *Crb1^{KO}Crb2$^{Low\text{-}imPRC}$* retina, the OLM showed disruptions (Fig. 2B, E and H). The *Crb1^{KO}Crb2$^{Low\text{-}imPRC}$* inferior retina showed frequent disruptions and loss of the OLM except for in the most-peripheral retina (Fig. 2C, F and I;Supplementary Material, Fig. S3). The *Crb1^{KO}Crb2$^{Low\text{-}imPRC}$* inferior retina showed a progressive loss of photoreceptor cells at the degenerative foci at 3 months (Fig. 2F;Supplementary Material, Fig. S4A) and 6 months of age (Fig. 2I;Supplementary Material, Fig. S4B). At 3 and 6 months of age abnormalities in the choroid and retinal blood vasculature became detectable (Fig. 2F and I, respectively). At 6 months of age, the *Crb1^{KO}Crb2$^{Low\text{-}imPRC}$* retinal pigment epithelium (RPE) layer and the inner retina including the ganglion cell layer (GCL) showed signs of degeneration (Fig. 2I). In the peripheral *Crb1^{KO}Crb2$^{Low\text{-}imPRC}$* inferior retina a sharp boundary between

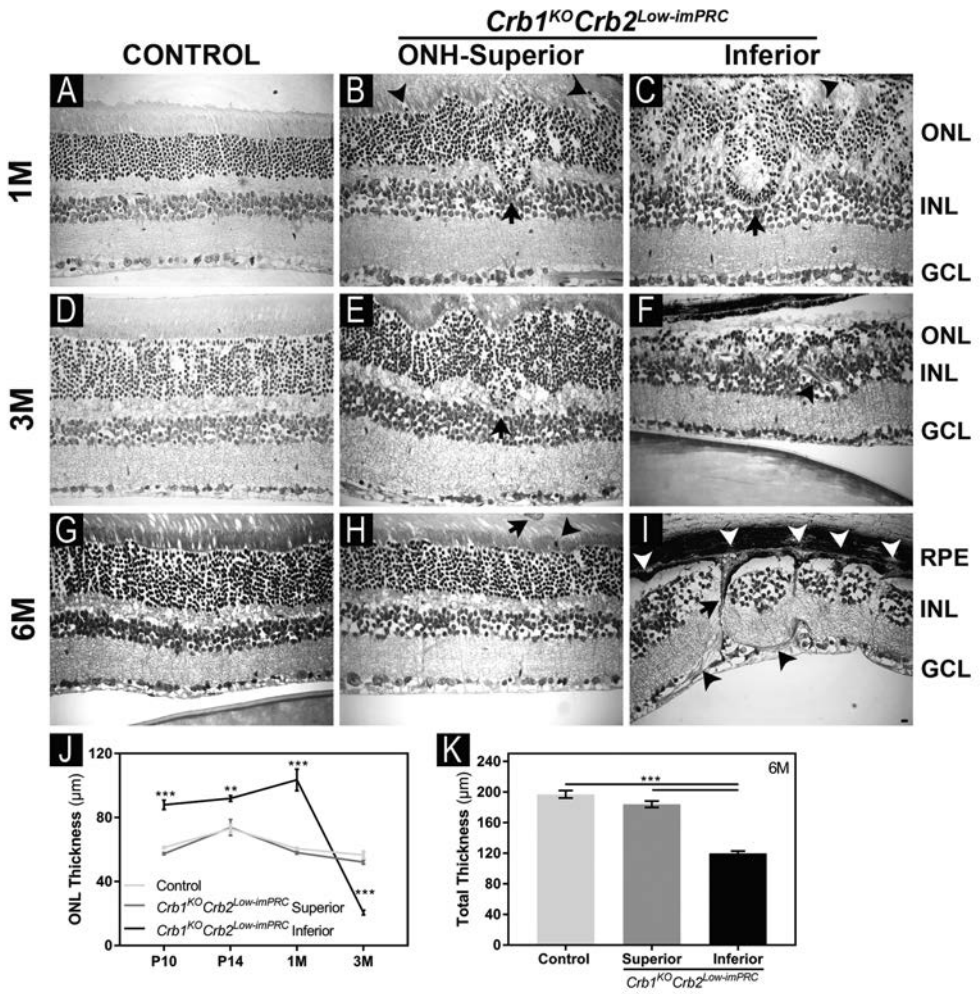

Figure 2. Removal of CRB1 from Müller glial cells and reduction of CRB2 from photoreceptors leads to abnormal layering and ONL thinning. Toluidine-stained light microscopy of retinal sections from control (A, D and G) and *Crb1*^{KO}*Crb2*$^{Low\text{-}imPRC}$ mice superior (B, E and H) and inferior (C, F and I), at different ages, (A–C)—1M, (D–F)—3M, (G–I)—6M. In the superior *Crb1*^{KO}*Crb2*$^{Low\text{-}imPRC}$ retina at 1-, 3-, and 6M of age, disruptions of the OLM, and protrusions of photoreceptor nuclei into the inner- and outer-segment layer (arrows), and ingressions of nuclei from the ONL into the OPL (arrowheads) are observed (B, E and H). In the inferior *Crb1*^{KO}*Crb2*$^{Low\text{-}imPRC}$ retina at 1M half rosettes in the ONL (arrowhead) and protrusions of INL cells into the ONL (arrow) are observed (C). In the inferior retina at 3M, there is thinning of the ONL (arrow) (F). At 3M and 6M there are areas with no ONL (arrowheads) (F and I). Quantification of ONL thickness in *Crb1*^{KO}*Crb2*$^{Low\text{-}imPRC}$ mice at 1 mm from the ONH showed significant thickening (P10, P14 and 1M) and thinning (3M) of the inferior versus the superior and control retina

(J). Total retina thickness at 6M was significantly thinner in the inferior versus superior and control retina (K). Scale bar: (A–I) 20 µm. Data are presented as mean ± SEM; $n = 3–4$, per timepoint. *$P < 0.05$; **$P < 0.01$, ***$P < 0.001$.

the area of phenotype and the area of the non-affected retina was observed at 1, 3 and 6 months of age (Supplementary Material, Fig. S5A–C). The spread of the *Crb1*^{KO}*Crb2*$^{Low\text{-}imPRC}$ inferior phenotype from the ONH to the peripheral inferior retina was variable between mice of the same age. The ONL in the inferior *Crb1*^{KO}*Crb2*$^{Low\text{-}imPRC}$ retinas was thickened at P10, P14, and 1 month of age and became thinned at 3 months of age, whereas the thickness of the ONL of the superior retina did not significantly change from P10 till 3 months of age (Fig. 2J). Total retinal thickness was decreased in the inferior versus superior *Crb1*^{KO}*Crb2*$^{Low\text{-}imPRC}$ retina and control retina at 6 months of age (Fig. 2K).

To further study the disruptions at the OLM observed in the histological analysis, we analysed the localization of proteins at the SAR (Fig. 3A–C: CRB2; Fig. 3D–F: PALS1; G–I: multiple-PDZ-protein MUPP1) and AJs (Fig. 3A–C: p120-catenin; Fig. 3D–F: N-cadherin,) by immunohistochemistry on 3-month-old control and *Crb1*^{KO}*Crb2*$^{Low\text{-}imPRC}$ retinas. In control retinas, we found SAR markers adjacent to AJs at the OLM (Fig. 3A, D and G). In the superior *Crb1*^{KO}*Crb2*$^{Low\text{-}imPRC}$ retina, the disruptions of the OLM were limited to the region immediately adjacent to the ONH, concomitant with the protrusion of photoreceptor nuclei into the inner- and outer-segment layer. The disruptions at foci at the OLM were confirmed by staining with markers of the SAR and AJs (Fig. 3B, E and H). In the inferior retina, at foci of degeneration the SAR and AJs were severely disrupted and showed at these foci loss of photoreceptors (Fig. 3C, F and I).

In control retina, SOX9-positive Müller glial cell nuclei reside in the inner nuclear layer (INL; Fig. 4A). Ectopic SOX9-positive Müller glial cell nuclei in the ONL further exemplified loss of conventional lamination in the 3-month-old *Crb1*^{KO}*Crb2*$^{Low\text{-}imPRC}$retina (Fig. 4B and C, arrows). In the affected areas, staining for glutamine synthetase appeared less regular especially apically at the OLM and in the ONL (Fig. 4B and C). The superior control retina showed localization of glial fibrillary acidic protein (GFAP) at the endfeet of Müller glial cells (Fig. 4D). *Crb1*^{KO}*Crb2*$^{Low\text{-}imPRC}$retina showed moderate upregulation of intermediate filament GFAP expression in Müller glial cells in the superior retina (Fig. 4E), this was even more pronounced in the inferior retina (Fig. 4F). In the *Crb1*^{KO}*Crb2*$^{Low\text{-}imPRC}$ inferior retina, GFAP expression was detected in apical processes wrapping around photoreceptors (Fig. 4F, arrow). Immunohistochemistry was performed to test whether the loss of retinal lamination in *Crb1*^{KO}*Crb2*$^{Low\text{-}imPRC}$ mice affected the retinal vasculature as well as infiltration of microglial cells. We stained with markers for activated (CD11b) and resting state (CD45) microglial cells and markers for endothelial cells and retinal vasculature such as Von Willebrand Factor (vWF) and Griffonia simplicifolia B4-isolectin (IB4). Microglial phagocytosis of living photoreceptors might contribute to retinal degeneration (48). In control retina, the microglial cells, the endothelial cells,

and vasculature were restricted to the inner retina (Fig. 4G and J). Abnormalities of the vasculature system were not observed at the superior side of the *Crb1*^{KO}*Crb2*$^{Low\text{-}imPRC}$retina close to the ONH (Fig. 4H and K). However, in the inferior retina abnormal neovascularization was detected (Fig. 4I and L). Ectopic localization of microglial cells was not observed at the superior side of the *Crb1*^{KO}*Crb2*$^{Low\text{-}imPRC}$ retina, but was detected close to the ONH (Fig. 4H and K) and even stronger at the inferior side of the retina (Fig. 4I and L). The data suggested ectopic hematopoietic and activated microglial cells in the degenerating *Crb1*^{KO}*Crb2*$^{Low\text{-}imPRC}$ photoreceptor layer. Interestingly, at some locations, the microglial cells, the hematopoietic cells and the endothelial cells were closely associated.

To test whether the severe disruption of the retinal lamination in 3-month-old *Crb1*^{KO}*Crb2*$^{Low\text{-}imPRC}$ retina had affected the photoreceptor synapses and the localization and structure of photoreceptors, we stained with several markers for photoreceptors. In the control retina (Fig. 5A), and the *Crb1*^{KO}*Crb2*$^{Low\text{-}imPRC}$ superior retina including close to the ONH, the inner retina and the outer retina appeared healthy (Fig. 5B). Whereas at the inferior side of the *Crb1*^{KO}*Crb2*$^{Low\text{-}imPRC}$ retina only a few photoreceptors were detected (Fig. 5C). In the *Crb1*^{KO}*Crb2*$^{Low\text{-}imPRC}$ inferior retina, the inner retina was relatively unaffected except for gaps of nuclei at foci in the INL (Fig. 5C). At the superior sides of control retina (Fig. 5D) and of the *Crb1*^{KO}*Crb2*$^{Low\text{-}imPRC}$ retina (data not shown), the rod and cone photoreceptor nuclei and inner and outer segments were orderly organized. Some photoreceptors protruded into the outer plexiform layer in the *Crb1*^{KO}*Crb2*$^{Low\text{-}imPRC}$ superior retina but only close to the ONH (Fig. 5E, boxed area). At the inferior side of the *Crb1*^{KO}*Crb2*$^{Low\text{-}imPRC}$ retina, only a few rod and cone photoreceptors survived (Fig. 5F). In the *Crb1*^{KO}*Crb2*$^{Low\text{-}imPRC}$ superior retina near the ONH, we found sporadic internalization of S-opsin which usually is expressed in the inner and outer segments of photoreceptors (Fig. 5G and H, boxed area). In the *Crb1*^{KO}*Crb2*$^{Low\text{-}imPRC}$ inferior retina, we found the loss of photoreceptor segments as marked by recoverin (Fig. 5C), internalized rhodopsin and S-opsin (Fig. 5I, boxed area).

The gaps in the INL presumably reside at areas where ectopic blood vessels pass through the INL (Figs 5C and 4L). Further analysis indicated that other inner retinal cell types such as PKCα-positive bipolar cells and calretinin-positive amacrine cells were not ectopically localized in the superior *Crb1*^{KO}*Crb2*$^{Low\text{-}imPRC}$ retina (Fig. 5A-B, J-Kand data not shown). In the *Crb1*^{KO}*Crb2*$^{Low\text{-}imPRC}$ inferior retina, nevertheless, bipolar cell dendrites were found protruding into the ONL (Fig. 5L). MPP4 is usually expressed at the synapses of photoreceptors being in a complex with other synaptic proteins such as PSD-95 and TMEM16b (49,50). In the control retina, photoreceptor synaptic proteins such as MPP4 localized at the outer plexiform layer (Fig. 5J). In the *Crb1*^{KO}*Crb2*$^{Low\text{-}imPRC}$ superior retina, photoreceptor synaptic proteins localized correctly and were detectable only at the outer plexiform layer (Fig. 5K), whereas in the *Crb1*^{KO}*Crb2*$^{Low\text{-}imPRC}$ inferior retina ectopic synapses were detected in the photoreceptor nuclear layer (NL; Fig. 5L).

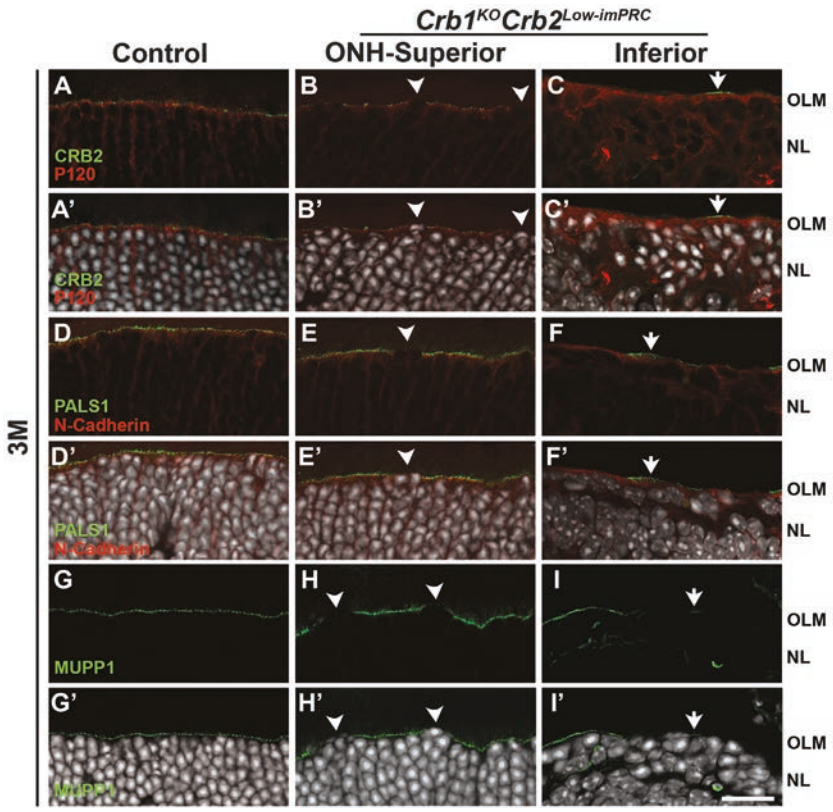

Figure 3. Maintenance of CRB complex in the adult *Crb1^{KO}Crb2$^{Low\text{-}imPRC}$* superior retina. CRB Complex in 3M *Crb1^{KO}Crb2$^{Low\text{-}imPRC}$* mice. Immunohistochemistry pictures from (3M) retina sections stained for SAR markers (red): CRB2 (A–C), PALS1 (D–F), MUPP1 (G–I) and for AJ markers (green): p120-catenin (A–C), N-cadherin (D–F). Disruptions of AJ markers were detected in both superior (B, E, H) and inferior (C, F, I) *Crb1^{KO}Crb2$^{Low\text{-}imPRC}$* retina. Ectopic photoreceptor nuclei protruded into the inner- and outer-segment layer in the superior *Crb1^{KO}Crb2$^{Low\text{-}imPRC}$* retina near the ONH were there were disruptions of SAR markers (B, E, H). Inferior *Crb1^{KO}Crb2$^{Low\text{-}imPRC}$* retina showed loss of SAR markers at phenotype foci but maintenance most peripherally. (C, F, I). A thickened apical OLM was positive for AJ markers in the inferior *Crb1^{KO}Crb2$^{Low\text{-}imPRC}$* retina at phenotype foci. Scale bar: 20 µm.

In summary, whereas we had previously shown that reduced levels of CRB2 in immature photoreceptors caused no retinal phenotype in the first five months (39), and that loss of CRB1 in progenitor and Müller glial cells caused a mild inferior-lateral retinal phenotype (30,37). Here, we suggest moderately reduced levels of CRB2 in immature photoreceptors with concomitant loss of CRB1 in progenitor and Müller glial cells results in a severe early-onset RP phenotype at the inferior side of the retina.

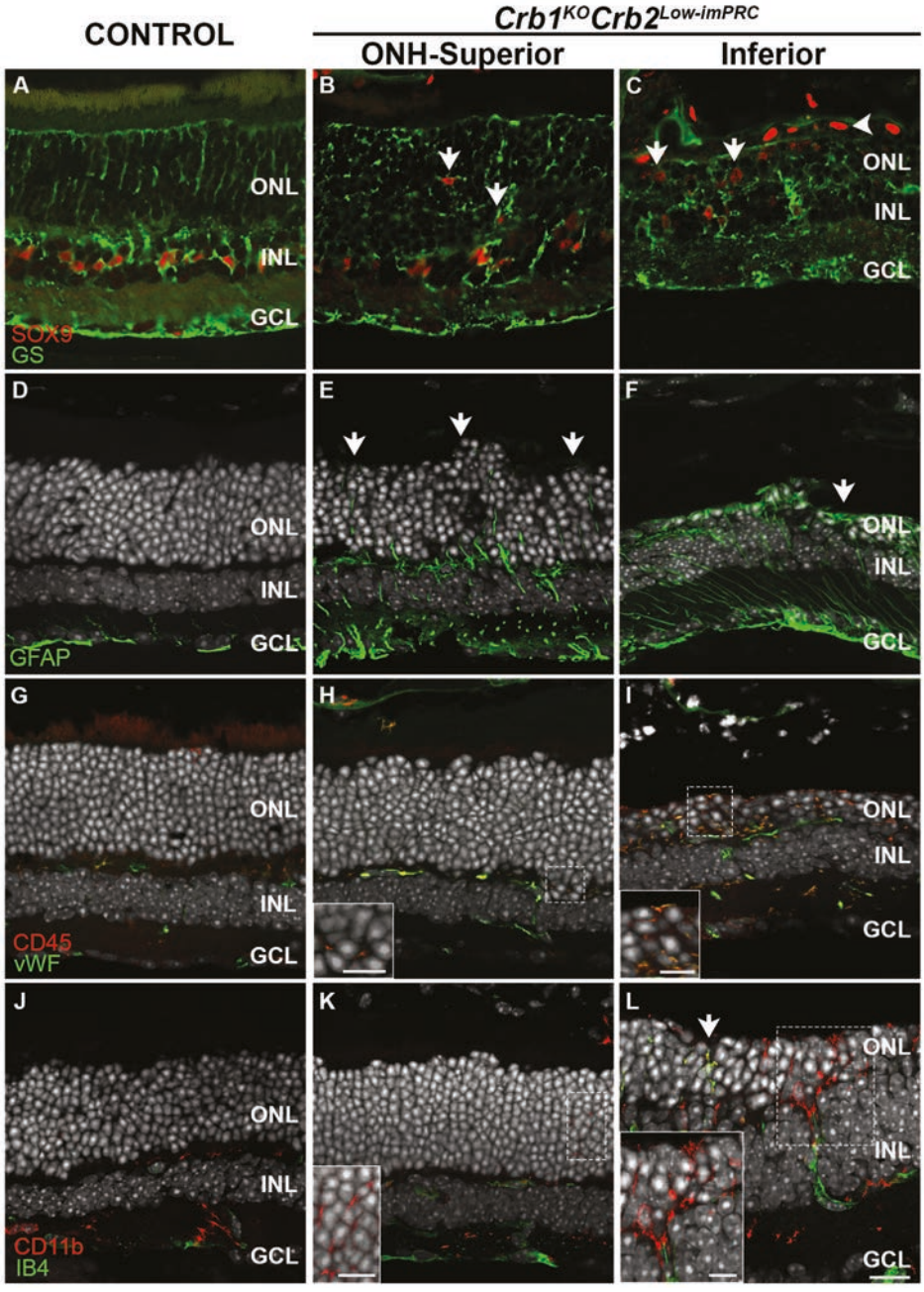
CONTROL
Crb1KO Crb2Low-imPRC
ONH-Superior
Inferior
A
B
C
ONL
INL
GCL
SOX9
GS
D
E
F
GFAP
G
H
I
CD45
vWF
J
K
L
CD11b
IB4

Figure 4. Neovascularization, gliosis and microglia activation due to lack of CRB1 in Müller glial cells and a decrease of CRB2 in photoreceptors. Immunohistochemistry of 3-month-old *Crb1^{KO}Crb2$^{Low\text{-}imPRC}$* mouse retinas. Sections were stained with antibodies against: SOX9 and glutamine synthetase (GS) (A–C), GFAP (D–F), CD45 and vWF (G–I), CD11b and IB4 (J–L). In the *Crb1^{KO}Crb2$^{Low\text{-}imPRC}$* retinas, SOX9-positive Müller glial cell nuclei were misplaced into the ONL both in the superior and inferior retina (arrows) (B and C). Arrowheads indicate the SOX9-positive nuclei in RPE. The *Crb1^{KO}Crb2$^{Low\text{-}imPRC}$* mutant retinas showed activated Müller glia cells, detected by an increase in the GFAP staining, more strongly inferiorly than superiorly (E and F). Activated apical processes were seen wrapping the OLM around photoreceptors (arrows) or INL cells (arrowhead) (E and F). An increase in microglial and endothelial cell markers in the ONL is observed more strongly inferiorly than superiorly in *Crb1^{KO}Crb2$^{Low\text{-}imPRC}$* retinas (H, I, K and L). CD45 and vWF primarily colocalized (inserts) being found more basally in the superior ONL and throughout the ONL inferiorly (H and I). CD11b was found to be expressed in the ONL (boxed area) or partially overlapped with IB4 (arrow) (K and L). Scale bars: (A–L) 20 µm, inserts in (H, I, K and L) 10 µm.

Loss of CRB2 in immature photoreceptors results in a phenotype that is more severe in the superior than in the inferior retina

Previously, we analysed retinas lacking CRB2 in immature rod and cone photoreceptors that developed an early RP phenotype because of the loss of photoreceptors throughout the retina (28). The retinas showed retinal disorganization of the photoreceptor layer with an overall proper lamination of the inner retina. In other studies, we analysed retinas lacking CRB1 and CRB2 specifically in immature radial glial progenitor cells that developed an LCA phenotype with overgrowth of late-born retinal cell types mimicking in part the thickened retina observed in patients with LCA due to loss of CRB1 (29,31). Here, we examined retinas lacking CRB1 with loss of CRB2 specifically in immature rod and cone photoreceptor cells and show these develop a novel LCA phenotype with thickened retina, without retinal overgrowth but with retinal redistribution of photoreceptors. No morphological defects were detected during early retinal development at embryonic day 13.5 (E13.5). Nevertheless disruptions at the OLM were detected from E15.5 in the *Crb1^{KO}Crb2$^{\Delta imPRC}$* mice as previously detected in *Crb2$^{\Delta imPRC}$* mice (39) (data not shown). From E17.5 onwards ectopic *Crb1^{KO}Crb2$^{\Delta imPRC}$* photoreceptor nuclei were detected in the GCL, half rosettes were found apically in the nuclear blast layer, and the lamination of the retina was significantly disturbed (Fig. 6B and C). Surprisingly, at E17.5 and P1, the *Crb1^{KO}Crb2$^{\Delta imPRC}$* superior retina shows a more severe phenotype with complete lack of OLM, whereas in the inferior retina there were still regions with an apparent intact OLM (Fig. 6B-C and E-F). Transmission electron microscopic analyses at E17.5 showed electron dense AJs in the control retina (Fig. 6J) but the loss of AJs in the *Crb1^{KO}Crb2$^{\Delta imPRC}$* retinas, as well as lack of inner segments and the appearance of ectopic nuclei close to the RPE (Fig. 6K). At P1 and P5 a distinct inner

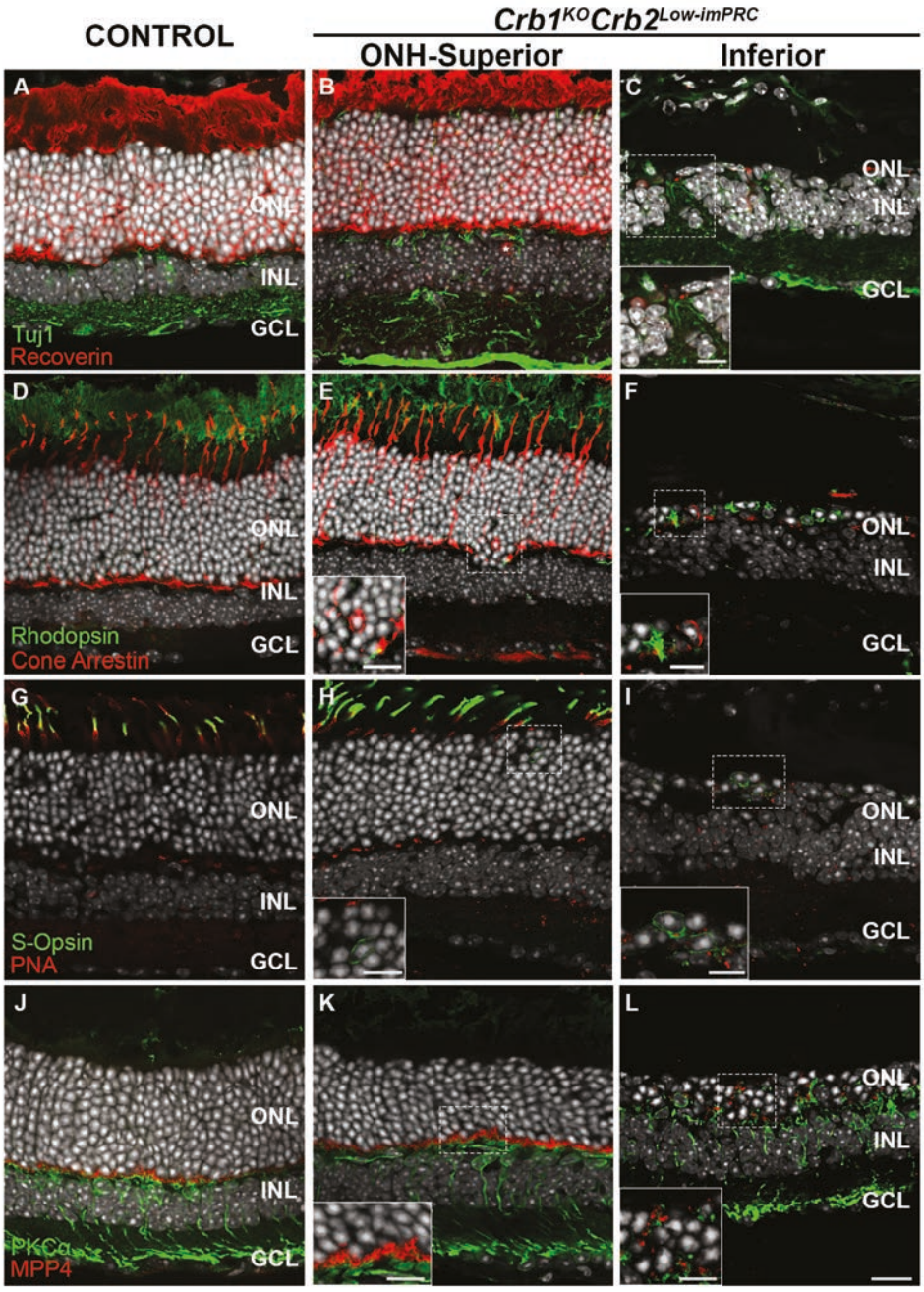
CONTROL
Crb1KO Crb2Low-imPRC
ONH-Superior
Inferior
A
B
C
ONL
INL
GCL
Tuj1
Recoverin
D
E
F
Rhodopsin
Cone Arrestin
G
H
I
S-Opsin
PNA
J
K
L
PKCα
MPP4

Figure 5. Reduction of CRB2 in photoreceptors and ablation of CRB1 from Müller glial cells leads to a disruption of synapses and degeneration of the photoreceptors. Immunohistochemistry of 3-month-old *Crb1^{KO}Crb2$^{Low\text{-}imPRC}$* mouse retinas. Sections were stained with antibodies against: Tuj1 and recoverin (A–C), rhodopsin and cone arrestin (D–F), S-opsin and PNA (G–I), PKCα and MPP4 (J–L). Recoverin positive cells localized to the ONL in Control (A) and superior *Crb1^{KO}Crb2$^{Low\text{-}imPRC}$* mouse retinas (B). Recoverin can also mark ON-bipolar cells, (asterisk, B). At foci in the inferior retina few photoreceptors remained and no longer had segments (C). Tuj1 normally localized to ganglion cells and dendrites in the superior *Crb1^{KO}Crb2$^{Low\text{-}imPRC}$* retina but could be found in breaks of the ONL/INL inferiorly (insert) (B and C). The *Crb1^{KO}Crb2$^{Low\text{-}imPRC}$* retina superiorly showed ectopic cones at basal positions (insert), and inferiorly at foci, few cones remained whiles ectopic rhodopsin expression was found in the cell soma (insert) (E and F). Superior and inferior *Crb1^{KO}Crb2$^{Low\text{-}imPRC}$* retina had ectopic S-opsin localized in the cell soma (inserts) (H and I). Mislocalized PNA positive staining was seen at foci of S-opsin internalization superiorly and throughout the ONL, INL, and GCL inferiorly (H and I). MPP4 was found mislocalized in the ONL, minorly superiorly and throughout degenerated foci inferiorly (inserts) (K and L). Protruding bipolar cell dendrites were found in the ONL inferiorly (arrow) (L). Scale bars: (A–L) 20 μm, inserts in (H, I, K and L) 10 μm.

plexiform layer and a GCL were formed in the *Crb1^{KO}Crb2$^{\Delta imPRC}$* retina. However, at the superior retina as well as at the inferior retina close to the ONH many ectopic nuclei resided in the GCL whereas less ectopic cells accumulated at the inferior side (Fig. 6E-F, H-I and L-M). In the control retina, the ONL, the outer plexiform layer (OPL), and the INL formed at P5 (Fig. 6G), although, in the *Crb1^{KO}Crb2$^{\Delta imPRC}$* retina, these layers fused to a single broad neuroblast layer (NBL) (Fig. 6H and I). Because the earliest observed effects were detected at the OLM, we analysed the SAR for disruptions using subapical markers CRB2, PAR3, PALS1, and MUPP1 and loss of AJ markers p120-catenin, β-catenin and N-cadherin. As expected from the earlier morphological analysis (Fig. 6E), the SAR and AJs were lost entirely in the *Crb1^{KO}Crb2$^{\Delta imPRC}$* superior retina (Fig. 7B, E, H and K) and the inferior retina close to the ONH (data not shown). In the morphologically less affected inferior retina (Fig. 6F), the SAR and AJs were detectable but showed disruptions at foci where nuclei protruded into the subretinal space (Fig. 7C, F, I and L).

Loss of CRB2 in immature photoreceptors affects mitosis and apoptosis

Previously we ablated either CRB2 or both CRB1 and CRB2 specifically in early retinal progenitors and their derived cells. In those retinas, we detected an increase in progenitor cells as well as late-born retinal cell types such as rod photoreceptors, bipolar cells, and Müller glial cells, and detected an increase in programmed cell death in the developing retina (28,29). The Crx-Cre transgenic mice used in the current study expressed Cre recombinase from E12.5 in immature postmitotic photoreceptors (46,51). In the *Crb1^{KO}Crb2$^{\Delta imPRC}$* retina, the Cre recombinase therefore ablated CRB2 in immature post-mitotic rod and cone photoreceptors but not in the retinal radial glial progenitor cells, whereas CRB1 was lost from radial glial

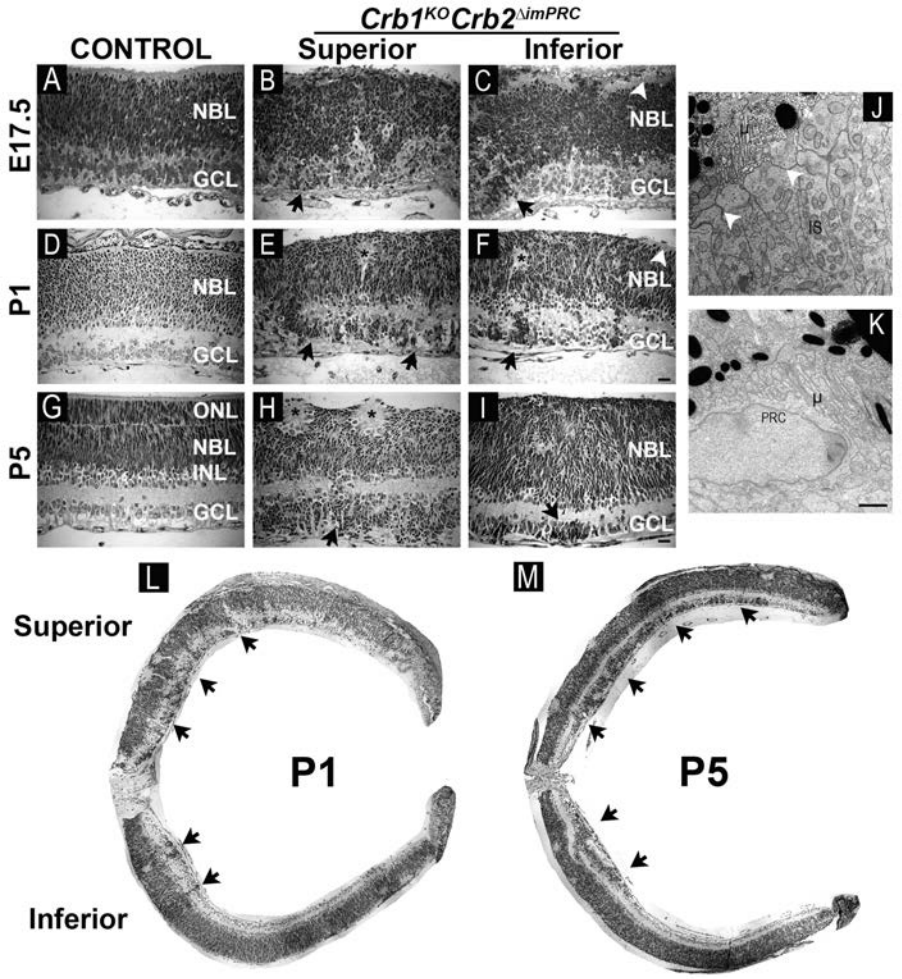

Figure 6. Severe and early retinal disorganization in *Crb1^{KO}Crb2^{ΔimPRC}* mice. Toluidine-stained light microscopy of retinal sections from control (A, D and G), superior (B, E and H) and inferior (C, F and I) *Crb1^{KO}Crb2^{ΔimPRC}* mice (at different ages, (A–C)—E17.5, (D–F, L)—P1, (G–I, M)—P5. Overview stitches of superior-inferior asymmetry in P1 and P5 *Crb1^{KO}Crb2^{ΔimPRC}* retina (L and M, respectively). In the *Crb1^{KO}Crb2^{ΔimPRC}* retina from E17.5 ectopic nuclei were found in the GCL (B and C, arrows). At E17 and P1 intact OLM is still present inferiorly (C and F, arrowheads). In P1 and P5 retina rosettes were found in the NL (E, F, and H, asterisk) and at P5 no separate ONL and OPL formed (H and I). Electron microscopic pictures of the SAR of retinal progenitor cells at E17.5 in control (J) and *Crb1^{KO}Crb2^{ΔimPRC}* retinas (K). In the control retina, the AJs were regularly distributed and aligned (J, arrowheads), and correct arrangement of photoreceptor inner segments were detected. In the *Crb1^{KO}Crb2^{ΔimPRC}* retina, AJs and inner segments were not observed (K). μ, microvilli; IS, inner segment; PRC, photoreceptor cell. Scale bars: (A–I) 20 μm, (J and K) 1 μm.

progenitor cells including all derived cells such as Müller glial cells that would typically express CRB1 (Supplementary Material, Fig. S1).

To check whether loss of CRB2 protein in immature post-mitotic photoreceptors affected the adjacent early retinal progenitors we stained for mitotic markers. Anti-phospho-histone H3 (anti-pH3) stains M-phase nuclei that reside most apically in the retina (Fig. 8A). Ectopic anti-pH3 positive nuclei were detected in the *Crb1^{KO}Crb2$^{\Delta imPRC}$* inner retina and the GCL at E17.5 and P1 (Fig. 8B, C and G). A significant increase in the total number of anti-pH3 positive nuclei was seen in *Crb1^{KO}Crb2$^{\Delta imPRC}$* retina when compared with *Crb1^{KO}Crb2$^{Low\text{-}imPRC}$* and control retina at P1 (Fig. 8G) but not at E17.5 (data not shown). Ki67 is a marker for cycling cells being expressed in G2, M, and the latter half of the S phase. In control developing retina, the newly formed GCL contained differentiated ganglion cells and displaced Starburst amacrine cells but no cycling cells (Fig. 8A, G and data not shown). In the *Crb1^{KO}Crb2$^{\Delta imPRC}$* retina, ectopic anti-Ki67 positive cells were detected in the GCL at E17.5 and P1 (Fig. 8B, C and H). Next, we checked whether or not there was an increase in the pool of progenitor cells, the total number of anti-Ki67 positive cells was not different from the *Crb1^{KO}Crb2$^{Low\text{-}imPRC}$* or control retina at P1 (Fig. 8H). We detected, however, an increase in the number of apoptotic cells at both E17.5 and P1 in *Crb1^{KO}Crb2$^{\Delta imPRC}$* retina (Fig. 8I and Supplementary Material, Fig. S4). In summary, loss of CRB1 from retinal progenitor cells with specific loss of CRB2 in immature photoreceptors resulted in an increased number of progenitors in M-phase concomitant with an increase in retinal cells undergoing programmed cell death.

Aberrant localization of photoreceptor cells in the inner retina and GCL of *Crb1^{KO}Crb2$^{\Delta imPRC}$* retina

To explore if the ectopic cycling cells in the inner retina had any effects on the localization of early-born post-mitotic photoreceptors cells, we stained post-mitotic photoreceptors with anti-recoverin. These cells were typically found most apically in P1 retina (Fig. 8D). We found an increased number of ectopic recoverin-positive cells in *Crb1^{KO}Crb2$^{\Delta imPRC}$* retina when compared with *Crb1^{KO}Crb2$^{Low\text{-}imPRC}$* and control retina at P1. These cells were localized at P1 in the bottom part of the NBL and the GCL (Fig. 8E and F).

The early developing *Crb1^{KO}Crb2$^{\Delta imPRC}$* retina showed differences in superior/inferior asymmetry in retinal dystrophy. Therefore we examined the P14 retina for thickness and localization of photoreceptor cells. Previously we did so for retinas lacking CRB1 and CRB2 in progenitor cells and found the ectopic localization of photoreceptors and inner retinal cells in the GCL. At P14 the ONL and INL in the *Crb1^{KO}Crb2$^{\Delta imPRC}$*retina were fused to a single NL of differentiated cells and lacked an outer plexiform layer, whereas this phenomenon was not detected in control or *Crb1^{KO}Crb2$^{Low\text{-}imPRC}$*retinas (Fig. 9A–C). Apically located rosettes of retinal cells were detectable in the most affected inferior part of the *Crb1^{KO}Crb2$^{Low\text{-}imPRC}$* retinas with low levels of CRB2, as well as in the superior and inferior parts of the

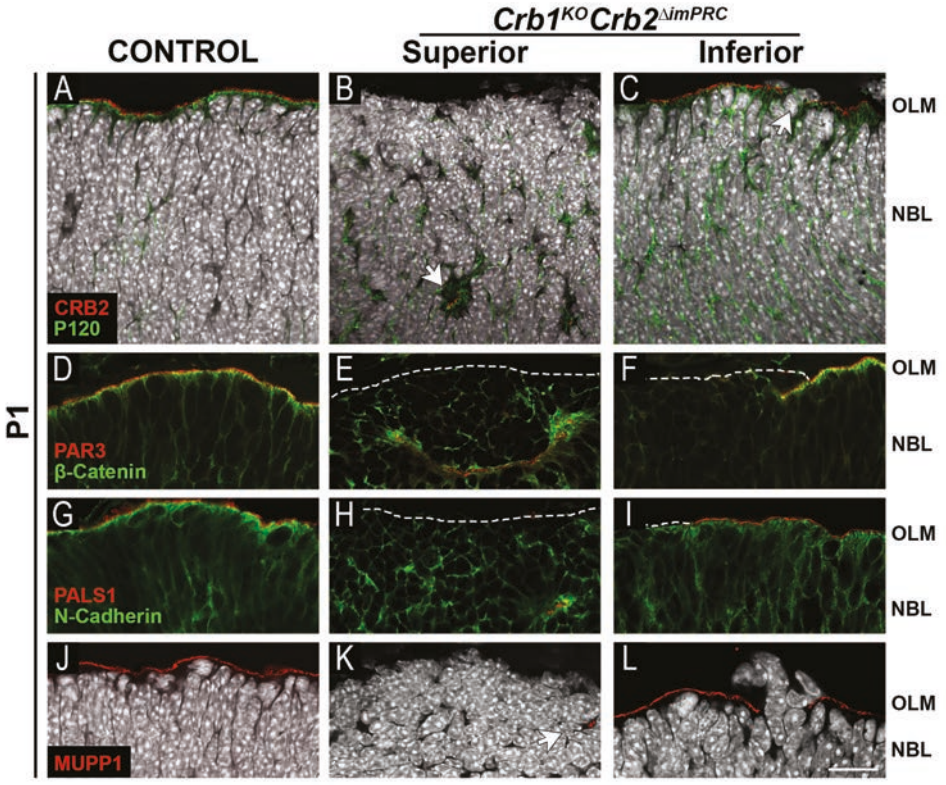

Figure 7. Peripheral inferior maintenance of CRB complex at the SAR in the early postnatal *Crb1^{KO}Crb2$^{\Delta imPRC}$* retina. Immunohistochemistry pictures from (P1) retina sections stained for SAR markers (red): CRB2 (A–C), PAR3 (D–F), PALS1 (G–I), MUPP1 (J–L) and for AJ markers (green): p120-catenin (A–C), β-catenin (D–F), N-cadherin (G–I). Disruptions of AJ markers were detected in both superior (B, E, H, K) and inferior (C, F, I, L) *Crb1^{KO}Crb2$^{\Delta imPRC}$* retina. SAR markers were mislocalized into the NBL in the superior *Crb1^{KO}Crb2$^{\Delta imPRC}$* retina (B, E, H, K). In the inferior *Crb1^{KO}Crb2$^{\Delta imPRC}$* peripheral retina SAR and AJ markers were found correctly localized in sections (C, F, I, L). Ectopic photoreceptor nuclei protruded into the inner- and outer-segment layer in the inferior *Crb1^{KO}Crb2$^{\Delta imPRC}$* retina (C and L). Scale bar: 20 µm.

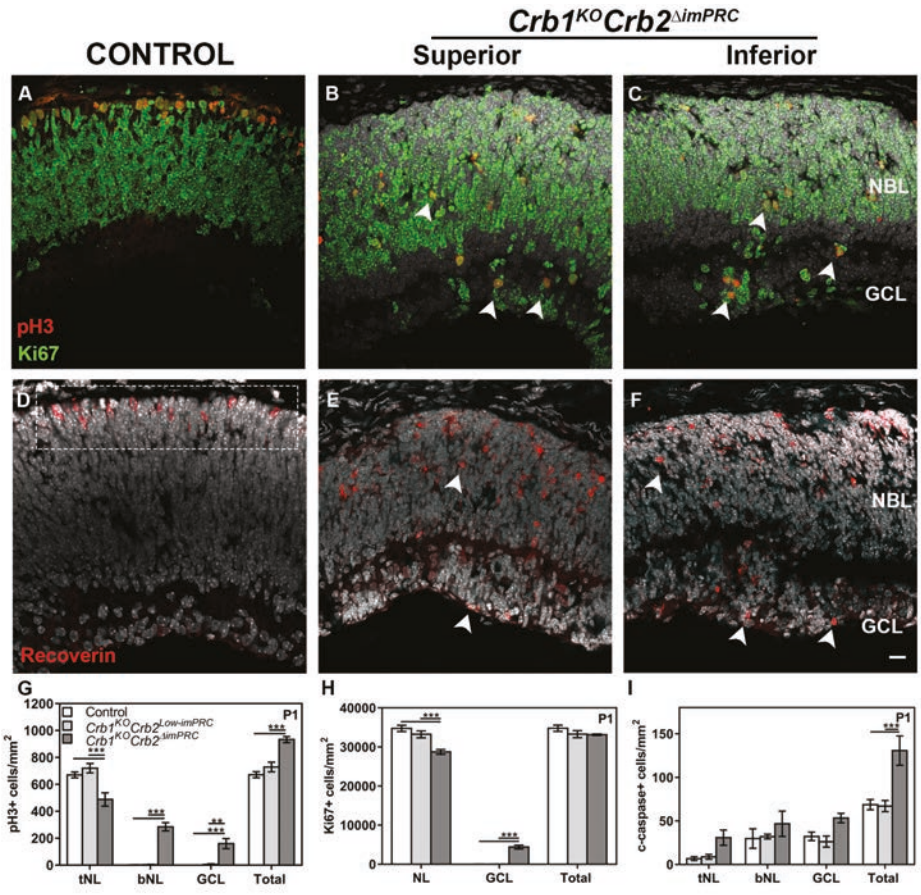

Figure 8. Lack of CRB2 from postmitotic photoreceptors and CRB1 from radial glial progenitors affects apoptosis and mitosis. Immunohistochemistry of P1 control (A and D), and *Crb1*^{KO}*Crb2*$^{\Delta imPRC}$superior (B and E) and inferior (C and F) mouse retinas. Sections were stained with antibodies against: Ki67 and pH3 (A–C), Recoverin (D–F). Quantification of pH3- (G), Ki67- (H) and cCaspase3-positive cells (I). Mislocalized pH3-positive dividing cells and Ki67-positive cycling cells were detected in the bNL and the GCL with an increase in total positive cells at P1 in *Crb1*^{KO}*Crb2*$^{\Delta imPRC}$ retina (B, C, arrowheads; quantifications G and H). Ectopic recoverin positive post-mitotic photoreceptors were found throughout the *Crb1*^{KO}*Crb2*$^{\Delta imPRC}$ retina (E and F, arrowheads). A significant increase in total apoptotic cells was found in *Crb1*^{KO}*Crb2*$^{\Delta imPRC}$ retina at P1 (I). tNL, top nuclear layer. Scale bar: (A–F) 20 µm. Data are presented as mean ± SEM; n = 3–4 retina, per genotype. *$P < 0.05$; **$P < 0.01$, ***$P < 0.001$.

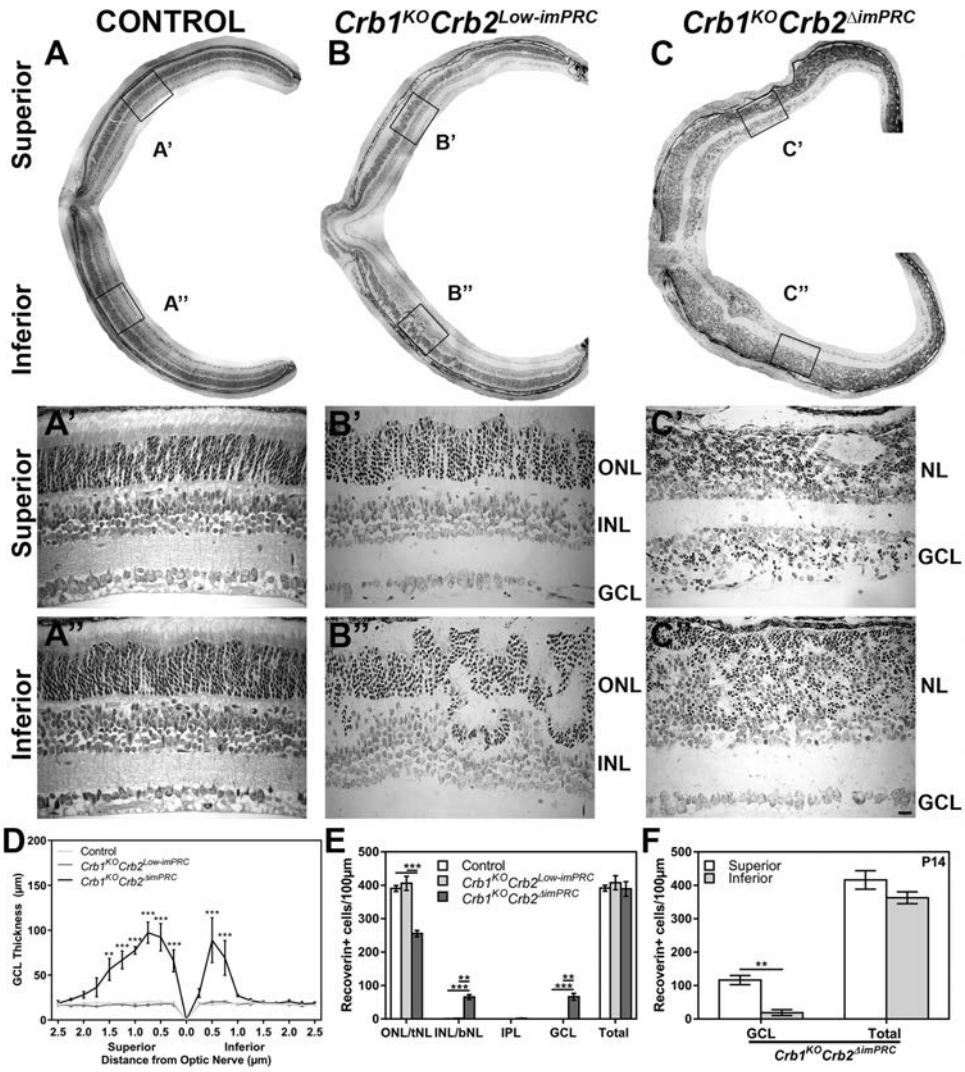

Figure 9. Conditional disruption of one or both alleles of *Crb2* in immature photoreceptors, on a genetic background lacking *Crb1*, leads to superior-inferior asymmetry. Toluidine-stained light microscopy showing retinal stitches (A–C) and superior (A′, B′ and C′) and inferior (A″, B″ and C″) inserts from control (A, A′ and A″), *Crb1*^{KO}*Crb2*$^{Low\text{-}imPRC}$ (B, B′ and B″) and *Crb1*^{KO}*Crb2*$^{\Delta imPRC}$ (C, C′ and C″) mice, at P14. Crb1^{KO}Crb2$^{Low\text{-}imPRC}$ retinas show an inferior phenotype of half rosettes in the ONL that ingressed into the INL at foci and ectopic photoreceptor nuclei that protruded into the inner- and outer-segment layer (B and B″). *Crb1*^{KO}*Crb2*$^{\Delta imPRC}$ retina exhibit a superior and inferior phenotype with apical rosettes, a single mixed NL abutting the RPE and ectopic photoreceptors in the GCL (C, C′ and C″). A significant increase in superior and inferior GCL thickness was found in *Crb1*^{KO}*Crb2*$^{\Delta imPRC}$retina

(D). GCL thickness was found to be extended further from the ONH superiorly than inferiorly. Quantification of recoverin-positive photoreceptor cells showed their mislocalization into the bNL and GCL of *Crb1^{KO}Crb2$^{\Delta imPRC}$* retina compared with *Crb1^{KO}Crb2$^{Low\text{-}imPRC}$* and control retina (E). A significantly higher amount of recoverin-positive photoreceptor cells were found in the superior compared with the inferior *Crb1^{KO}Crb2$^{\Delta imPRC}$* retina (F). . Scale bar: (A′, A″, B′, B″, C′ and C″) 20 µm. Data are presented as mean ± SEM; n = 3–4 retinae, per genotype. *$P < 0.05$; **$P < 0.01$, ***$P < 0.001$.

Crb1^{KO}Crb2$^{\Delta imPRC}$ retinas with loss of CRB2 (Fig. 9B″ and C). The GCL thickness was substantially increased in the inferior retina 0.75 mm from the ONH and in the entire superior retina in the *Crb1^{KO}Crb2$^{\Delta imPRC}$*. The GCL thickness was not changed in the inferior-peripheral retina of *Crb1^{KO}Crb2$^{\Delta imPRC}$* or the *Crb1^{KO}Crb2$^{Low\text{-}imPRC}$* or control retina (Fig. 9A–C, C″ and D). The increase in thickness in the GCL in the inferior side of *Crb1^{KO}Crb2$^{\Delta imPRC}$*retina was limited to the first 0.75 mm from the ONH whereas the most peripheral retina showed the normal thickness of the GCL (Fig. 9D, C and C″). The increase in thickness in the GCL at the superior side of the *Crb1^{KO}Crb2$^{\Delta imPRC}$* retina was limited to the first 1.5 mm from the ONH but being thicker closest to the ONH and thinning towards the peripheral retina (Fig. 9D). Staining for recoverin showed an increase in misplaced cells into the basal part of the NL (bNL) and GCL of P14 *Crb1^{KO}Crb2$^{\Delta imPRC}$*retina when compared with *Crb1^{KO}Crb2$^{Low\text{-}imPRC}$* or control retina (Fig. 9E). There was, however, not an increase in the total number of recoverin-positive cells. An increase in the number of ectopic recoverin-positive cells was found in the superior compared with the inferior *Crb1^{KO}Crb2$^{\Delta imPRC}$* retina (Fig. 9F). The ectopic photoreceptors were found to be mostly recoverin/rhodopsin double-positive rods, but mislocalized cones were also detected (Supplementary Material, Fig. S5). However, photoreceptor synaptic marker MPP4 could not be detected in the *Crb1^{KO}Crb2$^{Low\text{-}imPRC}$* retina at P14 (data not shown). Retinal neovascularization, as marked by IB4, was detected in the superior and inferior *Crb1^{KO}Crb2$^{\Delta imPRC}$* fused outer and inner NL, as well as in the outer NL in *Crb1^{KO}Crb2$^{Low\text{-}imPRC}$* mouse retina (Supplementary Material, Fig. S6).

DISCUSSION

In this study, we showed that (i) CRB2 levels in immature photoreceptors play a modulating role in determining the severities of CRB1 retinal dystrophies in mice; (ii) CRB2 plays essential roles in immature photoreceptors; (iii) loss of CRB2 localization at the SAR adjacent to AJs in immature photoreceptors disrupts the adhesion of immature retinal cell types at the OLM; (iv) CRB2 in immature photoreceptors determines the superior-inferior symmetry of the developing retina to maintain retinal structure and function; (v) physiological levels of CRB proteins in adjacent photoreceptors and Müller glial cells are essential for amelioration of CRB retinal dystrophies.

We showed here that levels of CRB2 in immature photoreceptors modulated CRB1 retinal dystrophies in mice. The data suggest CRB2 levels remaining in progenitor

cells and derived Müller glial cells were insufficient to maintain a laminated retinal structure in *Crb1^{KO}Crb2$^{\Delta imPRC}$* mouse retinas. Retinas lacking CRB1 and CRB2 in immature photoreceptors developed an LCA-like phenotype. We hypothesize patients with mutations in the *CRB1* gene with lowered levels or reduced function of CRB2 in immature photoreceptors will display a more severe phenotype than the ones with normal levels of CRB2 in photoreceptors. Recently, we showed CRB2 is present in foetal human radial glial progenitor cells in first-trimester retina, whereas CRB1 gets expressed from the second trimester coinciding with the birth of photoreceptors and Müller glial cells (52); unpublished data PQ and JW). The observed thickened retina, because of an increase in GCL thickness, in our *Crb1^{KO}Crb2$^{\Delta imPRC}$* mice might, therefore, mimic the thickened retina as found in LCA patients with mutations in the *CRB1* gene (12,13).

The retinal phenotype was attenuated from LCA to early-onset RP in the *Crb1^{KO}Crb2$^{Low\text{-}imPRC}$* mouse retinas with reduced levels of CRB2 in immature photoreceptors and full levels of CRB2 in progenitors and derived Müller glial cells. We propose maintenance of physiological levels of CRB proteins in adjacent photoreceptors and Müller glial cells are necessary for the amelioration of CRB retinal dystrophies.

In previous studies (39) we analysed retinas lacking CRB2 in immature retinas, *Crb2$^{\Delta imPRC}$* retinas. Here we detected a much more aggravated retinal phenotype in *Crb1^{KO}Crb2$^{\Delta imPRC}$* mice. The *Crb2$^{\Delta imPRC}$* retinas showed a phenotype throughout the entire retina without fusion of the outer and inner NLs mimicking early-onset RP, whereas the *Crb1^{KO}Crb2$^{\Delta imPRC}$* retinas showed a phenotype in which the outer and inner NLs fused throughout the entire retina mimicking LCA. Furthermore, in *Crb2$^{\Delta imPRC}$* retinas, we previously found sporadic abnormal localizations of photoreceptors in the GCL whereas in the *Crb1^{KO}Crb2$^{\Delta imPRC}$*retinas we found extensive mislocalization of photoreceptors in the GCL.

We hypothesize that CRB2 plays a critical role in maintaining adhesion between immature photoreceptors and progenitor cells besides a previously revealed role in E13.5—P5 retinal progenitors (29). In previous studies, we analysed retinas with loss of CRB2 as well as CRB1 in radial glial progenitors, which showed in part a similar retinal phenotype of LCA to the current studies on mice with loss of CRB2 in immature photoreceptors with concomitant loss of CRB1 from progenitor cells. Ablation of CRB2 or both CRB1 and CRB2 in cycling progenitors resulted in an increased number of progenitors with an increase in the number of late-born but not early-born retinal cell types (28,29). Our current data described an increase in the number of phospho-Histone H3 positive mitotic cells but no increase in the total progenitor pool at P1 in *Crb1^{KO}Crb2$^{\Delta imPRC}$* retinas compared with *Crb1^{KO}Crb2$^{Low\text{-}imPRC}$*retinas and control retinas. The increase in pH3-positive cells suggests a loss of CRB2 in immature photoreceptor cells caused an increased number of retinal progenitors in the M-phase of the cell cycle. The increased number of progenitors in M-phase did not result in a retina with an increased number of retinal cell types such as photoreceptors because of a concomitant increased programmed cell

death throughout the P1 retina. The similar early onset of disruptions at the OLM in *Crb1*^{KO}*Crb2*$^{\Delta imPRC}$ retinas compared with retinas lacking CRB2 and CRB1 in progenitors suggest a significant role for CRB2 in maintaining cellular adhesion in immature rod photoreceptors.

The early disruption of adhesion between immature retinal cell types at the OLM because of the loss of CRB2 in immature photoreceptors allows a testable working hypothesis on the pathologic steps towards LCA. The adherence junctions at the OLM with interactions of rod and cone photoreceptors with radial glial progenitor cells become disrupted, resulting in displaced rows of photoreceptors and ectopic half-rosettes. The ectopic half-rosettes contain immature photoreceptors as well as cycling progenitors produced at its regular location at the OLM. The ectopic cycling progenitors produced new immature photoreceptors in the nuclear blast layer, the GCL, or both. The displaced photoreceptors in the nuclear blast layer either stay there or migrate along radial glial progenitor cells or immature Müller glial cells towards the GCL. Alternatively, the ectopic photoreceptors are born in the GCL.

Previously, Jacobson *et al.* using optical coherence tomography, found that *CRB1*patient LCA retinas had 1.5 times thicker retina than normal and did not have the prototypic retinal layering. Interestingly, they identified a single combined NL and a broad inner retinal zone, which they hypothesized, would be a layer with increased ganglion cells among synaptic and glial elements (12). Moreover, a *CRB1* patient with Familial Foveal Retinoschisis, a rare autosomal recessive disorder typified by cart-wheel lesion restricted to the macula, was described having a thickened IPL-GCL, due to schitic changes of the retinal layers (18). We instead hypothesize that this broad inner retinal layer found in postnatal human *CRB1* LCA patients is similar to the thickened retina in *Crb1*^{KO}*Crb2*$^{\Delta imPRC}$ mice. Thus, being broader because of the displacement or the ectopic birth of photoreceptors in the inner retina.

Previously we have shown that in the adult wild-type retina CRB2 is expressed at higher levels in the inferior retina than in the superior retina, and CRB1 is expressed at higher levels in the superior retina than the inferior retina (31). Highlighting, opposing gradients of CRB1 and CRB2 expression. The CRB1 protein is expressed in the adult retina only in Müller glial cells (32). The CRB2 is expressed in the adult retina in both Müller glial cells and photoreceptors (32). The gradient of high levels of CRB2 at the OLM at the inferior side of the adult wild-type retina compared with the relatively low levels at the superior side does not inform about the relative levels of CRB2 at the SAR in Müller glial cells or photoreceptors. In the comparison of *Crb1*^{KO}*Crb2*$^{Low\text{-}imPRC}$ retinas to control retinas, we reduced levels of CRB2 in all immature photoreceptors and detected the spread of the phenotype from the superior side of the ONH to the peripheral inferior retina. From these data we hypothesize that the levels of CRB2 at the inferior side are at lower and more critical levels in immature photoreceptors than at the superior side of the retina, therefore causing severe retinal degeneration at the inferior side of the *Crb1*^{KO}*Crb2*$^{Low\text{-}imPRC}$retinas. We earlier suggested how variation of CRB2 levels in patients with mutations in the *CRB1* gene might affect the severity of the disease. Similarly, on the basis of clinical reports, we

hypothesize that variation of CRB2 levels affects spread of disease in *CRB1* patients. With some cases of LCA just affecting the inferior retina whiles other showing degeneration of all quadrants (12,14,22,53).

In the comparison of *Crb1*^{KO}*Crb2*$^{\Delta imPRC}$ retinas compared with *Crb1*^{KO}*Crb2*$^{Low\text{-}imPRC}$retinas we further reduced levels of CRB2 to null in immature photoreceptors and detected a more severe phenotype at the superior side than at the inferior side. The latter data suggest that upon complete loss of CRB2 in immature photoreceptors the remaining levels of CRB2 in the progenitors and Müller glial cells are not sufficient to maintain adhesion at the OLM between the various retinal cell types. We hypothesize therefore that CRB2 in immature photoreceptors determines the superior-inferior symmetry of the developing retina to maintain retinal structure and function. We have previously suggested that CRB2 is a modifier of the CRB1 retinal phenotype in mice and the modifier function of CRB2 also became apparent in the current study (31).

MATERIALS AND METHODS

Animals

Procedures concerning animals were performed with permission of the animal experimentation committee (DEC) of the Royal Netherlands Academy of Arts and Sciences (KNAW) and the ethical committee of the Leiden University Medical Center under permit number NIN 12.105. All mice used were maintained on a 100% C57BL/6JOlaHsd genetic background with a 12 h day–night cycle and supplied with food and water *ad libitum*. We crossed *Crb1–/–* mice (30) with *Crb2*$^{F/F}$Crx*Cre*$^{Tg/wt}$(*Crb2*$^{\Delta imPRC}$) (39) mice to obtain *Crb1–/–Crb2*$^{F/F}$Crx*CreTg/wt* (*Crb1*^{KO}*Crb2*$^{\Delta imPRC}$) and *Crb1–/–Crb2*$^{F/+}$Crx*CreTg/wt* (*Crb1*^{KO}*Crb2*$^{Low\text{-}imPRC}$) and Control *Crb1–/–Crb2*$^{F/+}$ and *Crb1–/–Crb2*$^{F/F}$ mice not expressing Cre. Subsequently, *Crb1*^{KO}*Crb2*$^{Low\text{-}imPRC}$ and *Crb1–/–Crb2*$^{F/F}$ mice were crossed to generate *Crb1*^{KO}*Crb2*$^{Low\text{-}imPRC}$, *Crb1*^{KO}*Crb2*$^{\Delta imPRC}$, and littermate Control mice. Analysis of *Crb1*^{KO}*Crb2*$^{\Delta imPRC}$ and *Crb1*^{KO}*Crb2*$^{Low\text{-}imPRC}$ mice was performed using only male animals. Chromosomal DNA isolation and genotyping were performed as described previously (28,39).

Electroretinography

Dark and light-adapted ERGs were performed under dim red light using an Espion E2 (Diagnosys, LLC, MA). ERGs were performed on 1-month-old (1M), 3M and 6M *Crb1*^{KO}*Crb2*$^{Low\text{-}imPRC}$ mice. Mice were anaesthetized using 100 mg/kg ketamine and 10 mg/kg xylazine intraperitoneally, and the pupils were dilated using atropine drops (5 mg/ml). Mice were placed on a temperature regulated heating pad, and reference and ground electrodes were placed subcutaneously in the scalp and the base of the tail, respectively. ERGs were recorded from both eyes using gold

wire electrodes. Hypromellose eye drops (3 mg/ml, Teva) were given between recordings to prevent eyes from drying. Single (Scotopic and Photopic ERG) or brief train (Flicker ERG) white (6500k)-flashes were used. Band-pass filter frequencies were 0.3 and 300 Hz. Scotopic recordings were obtained from dark-adapted animals at the following light intensities: –4, –3, –2, –1, 0, 1, 1.5 and 1.9 log cd s/m^2 (54). Flicker recordings were obtained under a fixed light intensity of 0.5 log cd s/m^2 with varying frequency (0.5, 1, 2, 3, 5, 7, 10, 12, 15, 18, 20 and 30 Hz) (55,56). Photopic recordings were performed following 10 min light adaptation on a background light intensity of 30 cd m^2 and the light intensity series used was: –2, –1, 0, 1, 1.5 and 1.9 log cd s/m^2 (54).

Morphological analysis

Eyes were collected at a range of time points from embryonic day E13.5 to 6M (n = 3–6/age/group). For morphological analysis, eyes were enucleated and fixed at room temperature with 4% paraformaldehyde in PBS for 20 min. After fixation, the eyes were dehydrated in 30, 50, 70, 90 and 100% ethanol for 30 min each. Eyes were orientated and embedded in Technovit 7100 (Kulzer, Wehrheim, Germany), according to the manufactures instructions and sectioned (3 µm). Slides were dried, counterstained with 0.5% toluidine blue and mounted under coverslips using Entellan (Merk, Darmstadt, Germany). Spidergrams of GCL thickness were measured every 250 µm from the ONH in P14 control, *Crb1*^{KO}*Crb2*$^{Low\text{-}imPRC}$ and *Crb1*^{KO}*Crb2*$^{\Delta imPRC}$mice (3 retinae per group (3 sections per retina)). ONL thickness was measured at 1 mm from the ONH in P10, P14, 1M and 3M *Crb1*^{KO}*Crb2*$^{Low\text{-}imPRC}$ retinas superiorly and inferiorly (3–4 retina per time point (3 sections per retina)). All bright field images were taken on Leitz DRMB microscope (Leica Microsystems).

Immunohistochemical analysis

For immunohistochemical analysis, eyes were incubated for 30 min in 4% paraformaldehyde in phosphate-buffered saline (PBS) for fixation and 5% and then 30% sucrose in PBS for cryo-protection. Finally, retinae were orientated, embedded in Tissue-Tek O.C.T Compound (Sakura, Finetek), frozen and stored at –20°C. Sections of 10 µm were made with a Leica CM1900 cryostat (Leica Microsystems). Sections for immunohistochemistry were blocked for 1 h in 10% normal goat serum, 0.4% Triton X-100 and 1% bovine serum albumin (BSA) in PBS, incubated in a moist-chamber overnight at 4°C primary antibodies were diluted in 0.3% normal goat serum, 0.4% Triton X-100 and 1% BSA in PBS. After rinsing in PBS, the sections were incubated for 1 h with complementary conjugated secondary antibodies and rinsed in PBS again. For quantification of dividing, cycling, and apoptotic cells retinal sections were stained with pH3 (E17.5 and P1), Ki67 (P1), and cleaved Caspase-3 (cCasp3) (E17.5 and P1) antibodies, respectively. Total numbers of cells were determined by manually counting antibody-positive cells per area on digital images (3–5 retinae

per time point (3–6 sections per retina)). P1 and P14 retinal sections were stained for quantification of photoreceptors (3–4 retinae per time point (3–6 sections per retina)).

Antibodies

The following primary antibodies were used: Sox9 (1:250; Millipore), glutamine synthetase (1:250; BD Biosciences), CD45 (1:100; eBioscience), vWF (1:100; Dako), CD11b (1:100; eBioscience), IB4 (1:100; Sigma), Tuj1 (1:200; Biolegend), Recoverin (1:500; Millipore), Rhodopsin (1:500; Millipore), Cone Arrestin (1:500; Millipore), S-opsin (1:250; Millipore), PNA (1:200; Vector Lab), PKCα (1:250; BD Biosciences), Ki67 (1:100; BD Biosciences), pH3 (1:100; Millipore), cCasp3 (1:250; Cell signalling), MPP4 AK4 (1:300; homemade) (30), MPP5/PALS1 SN47 (1:200; homemade), CRB1 AK2 (1:200; homemade) (30), CRB2 EP13 (1:200; homemade), MUPP1 (1:200; BD Biosciences), β-catenin (1:250; BD Biosciences), p120-catenin (1:250; BD Biosciences), GFAP (1:200; Dako), N-cadherin (1:250; BD Biosciences). Fluorescent-labelled secondary antibodies were rabbit anti-chicken, goat anti-mouse, goat anti-rabbit or goat anti-rat IgGs conjugated to Cy3 (1:500; Jackson Immunoresearch, Stanford, USA and Invitrogen), Alexa 488 or Alexa 555 (Abcam) or Dylight549. Sections were mounted in Vectashield HardSet DAPI mounting media (Vector Laboratories). A Leica DM6B fluorescence microscope and Leica TCS SP8 confocal microscope were used for Image acquisition. Image Analysis and processing were carried out using ImageJ and Adobe Photoshop CC2014.

Electron microscopy

Standard electron microscopy was performed as previously described (57). Eyes were fixed in 4% paraformaldehyde and 2% glutaraldehyde in PB for 24 h. They were rinsed in 0.1M sodium cacodylate buffered at pH 7.4 and postfixed for 2 h in 1% OsO_4 in 0.1M sodium cacodylate buffer (pH 7.4), containing 1.5% potassium ferricyanide. Eyes were embedded in epoxy resin and sections were cut, counterstained with uranyl acetate and lead citrate and examined in an FEI Tecnai electron microscope.

Statistical analysis

All statistical analyses were performed using GraphPad Prism version 7 (GraphPad Software). Normality of the distribution was tested by Kolmogorov–Smirnov test. Statistical significance was calculated by using *t*-test of 3–5 independent retinas/genotype/age. All values are expressed as mean ± SEM. Statistically significant values: $*P < 0.05$; $**P < 0.01$, $***P < 0.001$.

Acknowledgements
The authors thank Moira Goeman, Rawien Ramdien, Nynke van de Haar and Eline Nagel for technical assistance, Harald M. Mikkers and Monika Białecka for antibodies and all members of the Wijnholds Lab for advice on the manuscript.

Conflict of Interest statement. The LUMC is the holder of patent application PCT/NL2014/050549, which describes the potential clinical use of CRB2; J.W. is listed as the inventor on this patent, and J.W. is an employee of the LUMC.

Funding
Foundation Fighting Blindness: TA-GT-0313–0607-NIN, TA-GT-0715–0665-LUMC, The Netherlands Organisation for Health Research and Development: ZonMw grant 43200004, Curing Retinal Blindness Foundation, Stichting Retina Nederland Fonds, Landelijke St. Blinden en Slechtzienden, Rotterdamse Stichting, Blindenbelangen, St. Blindenhulp, St. Blinden-Penning, Algemene Nederlandse Vereniging ter Voorkoming van Blindheid (ANVVB), Gelderse Blinden Stichting and MaculaFonds.

REFERENCES

1 den Hollander, A.I., ten Brink, J.B., de Kok, Y.J., van Soest, S., van den Born, L.I., et al. (1999) Mutations in a human homologue of Drosophila crumbs cause retinitis pigmentosa (RP12). *Nat. Genet.*, 23, 217–221.

2 Richard, M., Roepman, R., Aartsen, W.M., van Rossum, A.G.S.H., den Hollander, et al. (2006) Towards understanding CRUMBS function in retinal dystrophies. *Hum. Mol. Genet.*, 15, R235–R243.

3 Quinn, P.M., Pellissier, L.P., Wijnholds, J. (2017) The CRB1 complex: following the trail of Crumbs to a feasible gene therapy strategy. *Front. Neurosci.*, 11, 175.

4 Verbakel, S.K., van Huet, R.A.C., Boon, C.J.F., den Hollander, A.I., Collin, R.W.J., et al. (2018) Non-syndromic retinitis pigmentosa. *Prog. Retin. Eye Res.*, 10.1016/j.preteyeres.2018.03.005.

5 Corton, M., Tatu, S.D., Avila-Fernandez, A., Vallespín, E., Tapias, I., et al. (2013) High frequency of CRB1 mutations as cause of Early-Onset Retinal Dystrophies in the Spanish population. *Orphanet. J. Rare Dis.*, 8, 20.

6 Vallespin, E., Cantalapiedra, D., Riveiro-Alvarez, R., Wilke, R., Aguirre-Lamban, J., et al. (2007) Mutation screening of 299 Spanish families with retinal dystrophies by Leber congenital amaurosis genotyping microarray. *Invest. Ophthalmol. Vis. Sci.*, 48, 5653–5661.

7 Talib, M., van Schooneveld, M.J., van Genderen, M.M., Wijnholds, J., Florijn, R.J., et al. (2017) Genotypic and phenotypic characteristics of CRB1-associated retinal dystrophies: a long-term follow-up study. *Ophthalmology*, 124, 884–895.

8 den Hollander, A.I., Roepman, R., Koenekoop, R.K., Cremers, F.P.M. (2008) Leber congenital amaurosis: genes, proteins and disease mechanisms. *Prog. Retin. Eye Res.*, 27, 391–419.

9 Hasan, S.M., Azmeh, A., Mostafa, O., Megarbane, A. (2016) Coat's like vasculopathy in leber congenital amaurosis secondary to homozygous mutations in CRB1: a case report and discussion of the management options. *BMC Res. Notes*, 9, 91.

10 Leber, T. (1869) Ueber Retinitis pigmentosa und angeborene Amaurose. *Albr. Von Graefes Arch. Klin. Exp. Ophthalmol.*, 15, 1–25.

11 Franceschetti, A., Dieterle, P. (1954) [Diagnostic and prognostic importance of the electroretinogram in tapetoretinal degeneration with reduction of the visual field and hemeralopia]. *Confin. Neurol.*, 14, 184–186

12 Jacobson, S.G., Cideciyan, A.V., Aleman, T.S., Pianta, M.J., Sumaroka, A., et al. (2003) Crumbs homolog 1 (CRB1) mutations result in a thick human retina with abnormal lamination. *Hum. Mol. Genet.*, 12, 1073–1078.

13 Aleman, T.S., Cideciyan, A.V., Aguirre, G.K., Huang, W.C., Mullins, et al. (2011) Human CRB1-associated retinal degeneration: comparison with the rd8 Crb1-mutant mouse model. *Invest. Ophthalmol. Vis. Sci.*, 52, 6898–6910.

14 McKay, G.J., Clarke, S., Davis, J.A., Simpson, D.A.C., Silvestri, G. (2005) Pigmented paravenous chorioretinal atrophy is associated with a mutation within the crumbs homolog 1 (CRB1) gene. *Invest. Ophthalmol. Vis. Sci.*, 46, 322–328.

15 Simonelli, F., Ziviello, C., Testa, F., Rossi, S., Fazzi, E., et al. (2007) Clinical and molecular genetics of Leber's congenital amaurosis: a multicenter study of Italian patients. *Invest. Opthalmol. Vis. Sci.*, 48, 4284–4290.

16 Heckenlively, J.R. (1982) Preserved para-arteriole retinal pigment epithelium (PPRPE) in retinitis pigmentosa. *Br. J. Ophthalmol.*, 66, 26–30.
17 den Hollander, A.I., Heckenlively, J.R., van den Born, L.I., de Kok, Y.J.M., van der Velde-Visser, et al. (2001) Leber congenital amaurosis and retinitis pigmentosa with Coats-like exudative vasculopathy are associated with mutations in the crumbs homologue 1 (CRB1) gene. *Am. J. Hum. Genet.*, 69, 198–203.
18 Vincent, A., Ng, J., Gerth-Kahlert, C., Tavares, E., Maynes, J.T., et al. (2016) Biallelic mutations in CRB1 underlie autosomal recessive familial foveal retinoschisis. *Invest. Ophthalmol. Vis. Sci.*, 57, 2637–2646.
19 Zenteno, J.C., Buentello-Volante, B., Ayala-Ramirez, R., Villanueva-Mendoza, C. (2011) Homozygosity mapping identifies the Crumbs homologue 1 (Crb1) gene as responsible for a recessive syndrome of retinitis pigmentosa and nanophthalmos. *Am. J. Med. Genet. A*, 155, 1001–1006.
20 McMahon, T.T., Kim, L.S., Fishman, G.A., Stone, E.M., Zhao, X.C., et al. (2009) CRB1 gene mutations are associated with keratoconus in patients with leber congenital amaurosis. *Invest. Ophthalmol. Vis. Sci.*, 50, 3185–3187.
21 Lotery, A.J., Malik, A., Shami, S.A., Sindhi, M., Chohan, et al. (2001) CRB1 mutations may result in retinitis pigmentosa without para-arteriolar RPE preservation. *Ophthalmic Genet.*, 22, 163–169.
22 Khan, K.N., Robson, A., Mahroo, O.A.R., Arno, G., Inglehearn, C.F., et al. (2018) A clinical and molecular characterisation of CRB1-associated maculopathy. *Eur. J. Hum. Genet.*, doi:10.1038/s41431-017-0082-2.
23 Tsang, S.H., Burke, T., Oll, M., Yzer, S., Lee, W., et al. (2014) Whole exome sequencing identifies CRB1 defect in an unusual maculopathy phenotype. *Ophthalmology*, 121, 1773–1782.
24 Bulgakova, N.A., Knust, E. (2009) The Crumbs complex: from epithelial-cell polarity to retinal degeneration. *J. Cell Sci.*, 122, 2587–2596.
25 Bachmann, A., Schneider, M., Theilenberg, E., Grawe, F., Knust, E. (2001) Drosophila Stardust is a partner of Crumbs in the control of epithelial cell polarity. *Nature*, 414, 638–643.
26 Lemmers, C., Michel, D., Lane-Guermonprez, L., Delgrossi, M.-H., Médina, E., et al. (2004) CRB3 binds directly to Par6 and regulates the morphogenesis of the tight junctions in mammalian epithelial cells. *Mol. Biol. Cell*, 15, 1324–1333.
27 Roh, M.H., Makarova, O., Liu, C.J., Shin, K., Lee, S., et al. (2002) The Maguk protein, Pals1, functions as an adapter, linking mammalian homologues of crumbs and discs lost. *J. Cell Biol.*, 157, 161–172.
28 Alves, C.H., Sanz, A.S., Park, B., Pellissier, L.P., Tanimoto, N., et al. (2013) Loss of CRB2 in the mouse retina mimics human retinitis pigmentosa due to mutations in the CRB1 gene. *Hum. Mol. Genet.*, 22, 35–50.
29 Pellissier, L.P., Alves, C.H., Quinn, P.M., Vos, R.M., Tanimoto, N., et al. (2013) Targeted ablation of CRB1 and CRB2 in retinal progenitor cells mimics Leber congenital amaurosis. *PLoS Genet.*, 9, e1003976.
30 van de Pavert, S. A., Kantardzhieva, A., Malysheva, A., Meuleman, J., Versteeg, I., et al. (2004) Crumbs homologue 1 is required for maintenance of photoreceptor cell polarization and adhesion during light exposure. *J. Cell Sci.*, 117, 4169–4177.
31 Pellissier, L.P., Lundvig, D.M.S., Tanimoto, N., Klooster, J., Vos, R.M., et al. (2014) CRB2 acts as a modifying factor of CRB1-related retinal dystrophies in mice. *Hum. Mol. Genet.*, 23, 3759–3771.

32 van Rossum, A.G.S.H., Aartsen, W.M., Meuleman, J., Klooster, J., Malysheva, A., et al. (2006) Pals1/Mpp5 is required for correct localization of Crb1 at the subapical region in polarized Muller glia cells. *Hum. Mol. Genet.*, 15, 2659–2672.

33 Zou, J., Wang, X., Wei, X. (2012) Crb apical polarity proteins maintain zebrafish retinal cone mosaics via intercellular binding of their extracellular domains. *Dev. Cell*, 22, 1261–1274.

34 Pellissier, L.P., Quinn, P.M., Alves, C.H., Vos, R.M., Klooster, et al. (2015) Gene therapy into photoreceptors and Müller glial cells restores retinal structure and function in CRB1 retinitis pigmentosa mouse models. *Hum. Mol. Genet.*, 24, 3104–3118.

35 den Hollander, A.I., Ghiani, M., de Kok, Y.J.M., Wijnholds, J., Ballabio, A., et al. (2002) Isolation of Crb1, a mouse homologue of Drosophila crumbs, and analysis of its expression pattern in eye and brain. *Mech. Dev.*, 110, 203–207.

36 Alves, C.H., Pellissier, L.P., Wijnholds, J. (2014) The CRB1 and adherens junction complex proteins in retinal development and maintenance. *Prog. Retin. Eye Res.*, 40, 35–52.

37 van de Pavert, S.A., Sanz, A.S., Aartsen, W.M., Vos, R.M., Versteeg, I., et al. (2007) Crb1 is a determinant of retinal apical Müller glia cell features. *Glia*, 55, 1486–1497.

38 van de Pavert, S. A., Meuleman, J., Malysheva, A., Aartsen, W.M., Versteeg, I., et al. (2007) A single amino acid substitution (Cys249Trp) in Crb1 causes retinal degeneration and deregulates expression of pituitary tumor transforming gene Pttg1. *J. Neurosci.*, 27, 564–573.

39 Alves, C.H., Pellissier, L.P., Vos, R.M., Garcia Garrido, M., Sothilingam, V., et al. (2014) Targeted ablation of Crb2 in photoreceptor cells induces retinitis pigmentosa. *Hum. Mol. Genet.*, 23, 3384–3401.

40 Zhao, M., Andrieu-Soler, C., Kowalczuk, L., Paz Cortés, M., Berdugo, M., et al. (2015) A new CRB1 rat mutation links Müller glial cells to retinal telangiectasia. *J. Neurosci.*, 35, 6093–6106.

41 Mehalow, A.K., Kameya, S., Smith, R.S., Hawes, N.L., Denegre, J.M., et al. (2003) CRB1 is essential for external limiting membrane integrity and photoreceptor morphogenesis in the mammalian retina. *Hum. Mol. Genet.*, 12, 2179–2189.

42 Alves, C.H., Bossers, K., Vos, R.M., Essing, A.H.W., Swagemakers, S., et al. (2013) Microarray and morphological analysis of early postnatal CRB2 mutant retinas on a pure C57BL/6J genetic background. *PLoS One*, 8, e82532.

43 Dudok, J.J., Sanz, A.S., Lundvig, D.M.S., Sothilingam, V., Garrido, M.G., et al. (2013) MPP3 regulates levels of PALS1 and adhesion between photoreceptors and Müller cells. *Glia*, 61, 1629–1644.

44 Park, B., Alves, C.H., Lundvig, D.M., Tanimoto, N., Beck, S.C., et al. (2011) PALS1 is essential for retinal pigment epithelium structure and neural retina stratification. *J. Neurosci.*, 31, 17230–17241.

45 Bujakowska, K., Audo, I., Mohand-Saïd, S., Lancelot, M.-E., Antonio, A., et al. (2012) CRB1 mutations in inherited retinal dystrophies. *Hum. Mutat.*, 33, 306–315.

46 Koike, C., Nishida, A., Akimoto, K., Nakaya, M., Noda, T., et al. (2005) Function of atypical protein kinase C lambda in differentiating photoreceptors is required for proper lamination of mouse retina. *J. Neurosci.*, 25, 10290–10298.

47 Park, R., Moon, U.Y., Park, J.Y., Hughes, L.J., Johnson, R.L., et al. (2016) Yap is required for ependymal integrity and is suppressed in LPA-induced hydrocephalus. *Nat. Commun.*, 7, 10329.

48 Zhao, L., Zabel, M.K., Wang, X., Ma, W., Shah, P., et al. (2015) Microglial phagocytosis of living photoreceptors contributes to inherited retinal degeneration. *EMBO Mol. Med.*, 7, 1179–1197.

49 Aartsen, W.M., Kantardzhieva, A., Klooster, J., van Rossum, A.G.S.H., van de Pavert, S.A., et al. (2006) Mpp4 recruits Psd95 and Veli3 towards the photoreceptor synapse. *Hum. Mol. Genet*., 15, 1291–1302.

50 Stöhr, H., Heisig, J.B., Benz, P.M., Schöberl, S., Milenkovic, V.M., et al. (2009) TMEM16B, a novel protein with calcium-dependent chloride channel activity, associates with a presynaptic protein complex in photoreceptor terminals. *J. Neurosci.*, 29, 6809–6818.

51 Nishida, A., Furukawa, A., Koike, C., Tano, Y., Aizawa, S., et al. (2003) Otx2 homeobox gene controls retinal photoreceptor cell fate and pineal gland development. *Nat. Neurosci.*, 6, 1255–1263.

52 Quinn, P.M., Buck, T.M., Alves, C., Ohonin, C., Chuva de Sousa Lopes, S.M., et al. (2017) Recapitulation of the human fetal crumbs complex in human iPSCs-derived retinas and retinal pigment epithelium. *Invest. Ophthalmol. Vis. Sci.*, 58, 3758.

53 Yzer, S., Fishman, G.A., Racine, J., Al-Zuhaibi, S., Chakor, H., Dorfman, A., et al. (2006) CRB1 heterozygotes with regional retinal dysfunction: implications for genetic testing of leber congenital amaurosis. *Invest. Ophthalmol. Vis. Sci.*, 47, 3736–3744.

54 Nishiguchi, K.M., Carvalho, L.S., Rizzi, M., Powell, K., Holthaus, S.-M.K., et al. (2015) Gene therapy restores vision in rd1 mice after removal of a confounding mutation in Gpr179. *Nat. Commun.*, 6, 6006.

55 Tanimoto, N., Sothilingam, V., Kondo, M., Biel, M., Humphries, P., et al. (2015) Electroretinographic assessment of rod- and cone-mediated bipolar cell pathways using flicker stimuli in mice. *Sci. Rep.*, 5, 10731.

56 Tanimoto, N., Akula, J.D., Fulton, A.B., Weber, B.H.F., et al. (2016) Differentiation of murine models of 'negative ERG' by single and repetitive light stimuli. *Doc. Ophthalmol.*, 132, 101–109.

57 Klooster, J., Kamermans, M. (2016) An ultrastructural and immunohistochemical analysis of the outer plexiform layer of the retina of the European silver eel (Anguilla anguilla L). *PLoS One*, 11, e0152967–e0152921.

SUPPLEMENTARY FIGURES AND LEGENDS

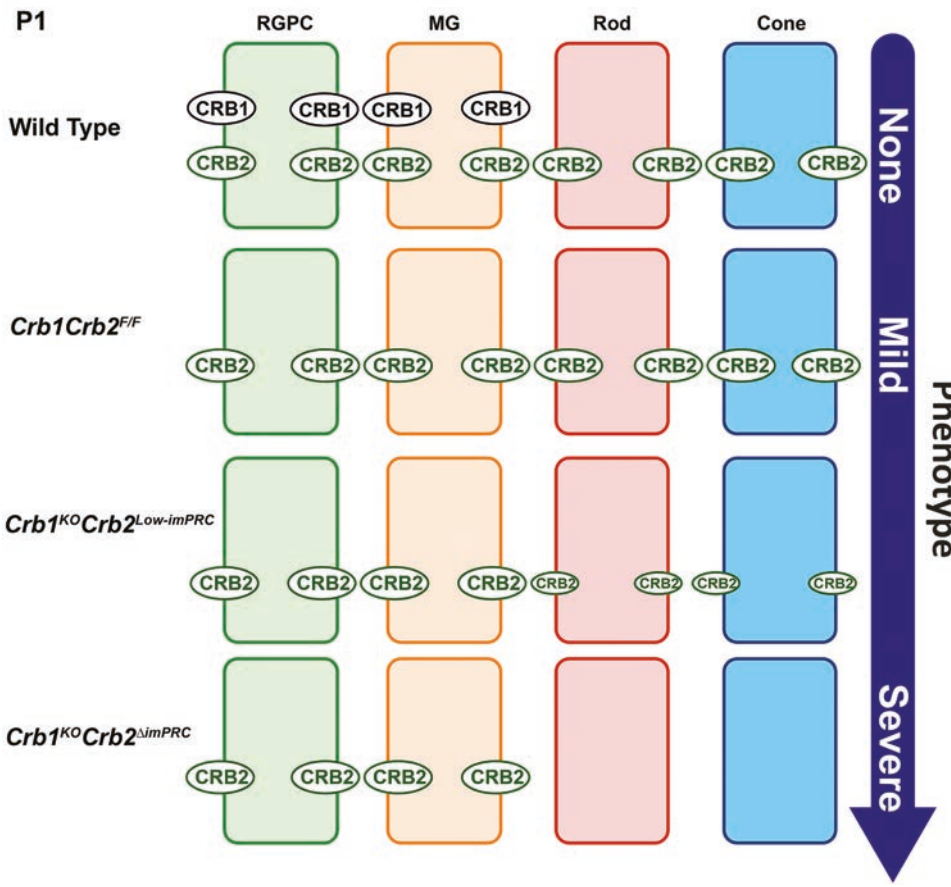

Supplemental Figure 1: Graphical schematic of the localisation of CRB1 and CRB2 in radial glial progenitor cells (RGPC), Müller glial cells (MG), Rod and Cone photoreceptor cells in wild-type, *Crb1Crb2*$^{F/F}$ (Control), *Crb1*^{KO}*Crb2*$^{Low\text{-}imPRC}$, and *Crb1*^{KO}*Crb2*$^{\Delta imPRC}$ mice.

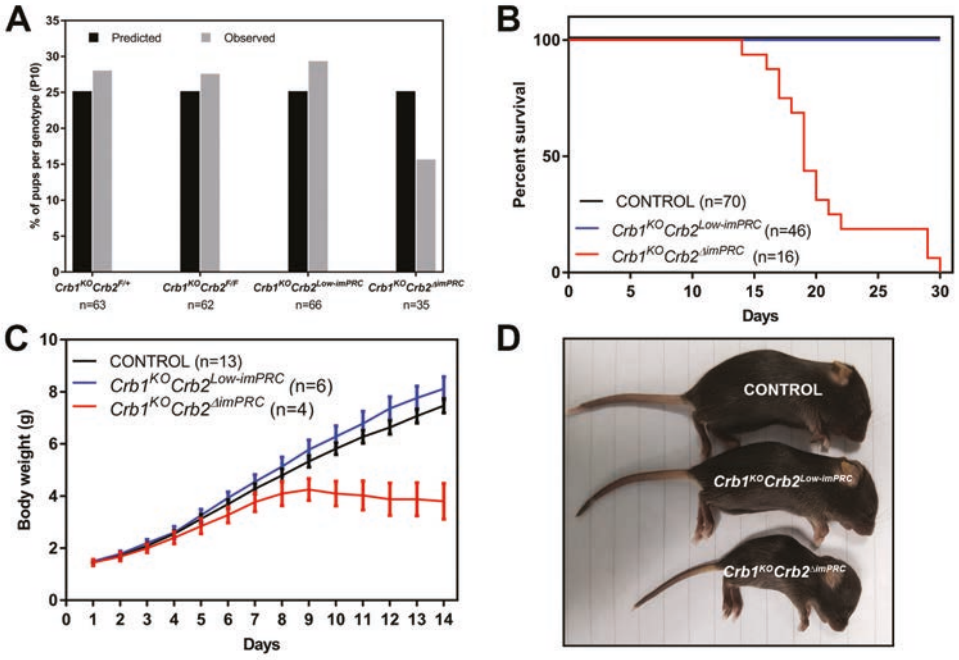

Supplemental Figure 2: Reduced *Mendelian* ratio, survival, and body weight in *Crb1^{KO}Crb2$^{\Delta imPRC}$* mice with hydrocephalus. Lower than the predicted Mendelian ratio of *Crb1^{KO}Crb2$^{\Delta imPRC}$* mice (A). Reduced percent survival of *Crb1^{KO}Crb2$^{\Delta imPRC}$* mice compared to *Crb1^{KO}Crb2$^{Low\text{-}imPRC}$* and control mice (B). *Crb1^{KO}Crb2$^{\Delta imPRC}$* mice unable to sustain their body weight compared to *Crb1^{KO}Crb2$^{Low\text{-}imPRC}$* and control mice (C). Picture of P14 control, *Crb1^{KO}Crb2$^{Low\text{-}imPRC}$*, and *Crb1^{KO}Crb2$^{\Delta imPRC}$* mice. *Crb1^{KO}Crb2$^{\Delta imPRC}$* mouse has hydrocephalus.

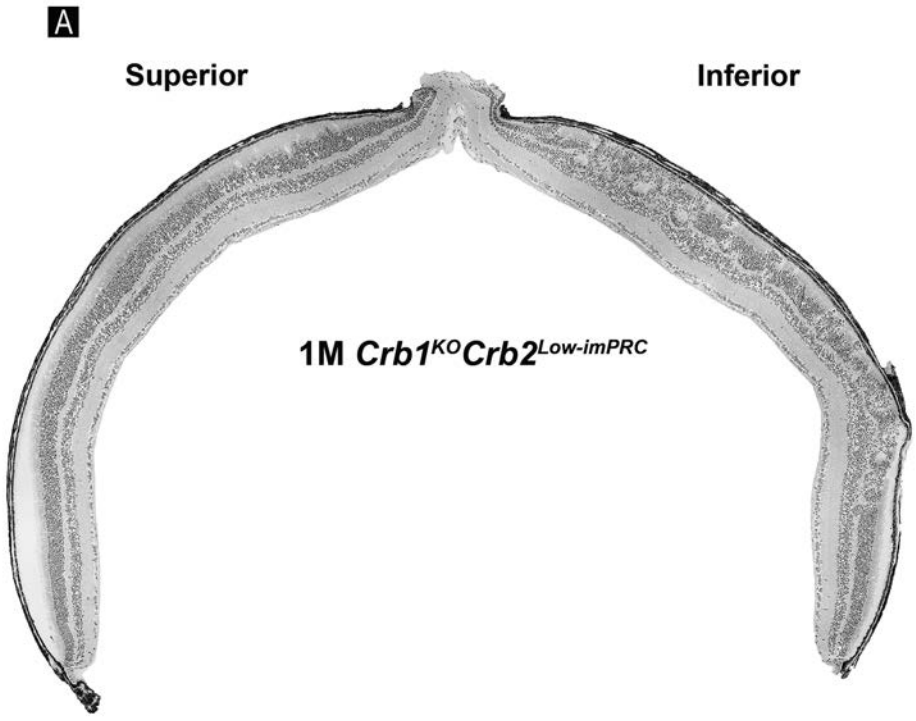

Supplemental Figure 3: Abnormal layering and superior/inferior asymmetry in adult *Crb1^{KO}Crb2$^{Low-imPRC}$* mice. Toluidine-stained light microscopy (A). Retinal stitch of 1M *Crb1^{KO}Crb2$^{\Delta imPRC}$* mouse retina showing superior- inferior asymmetry (A).

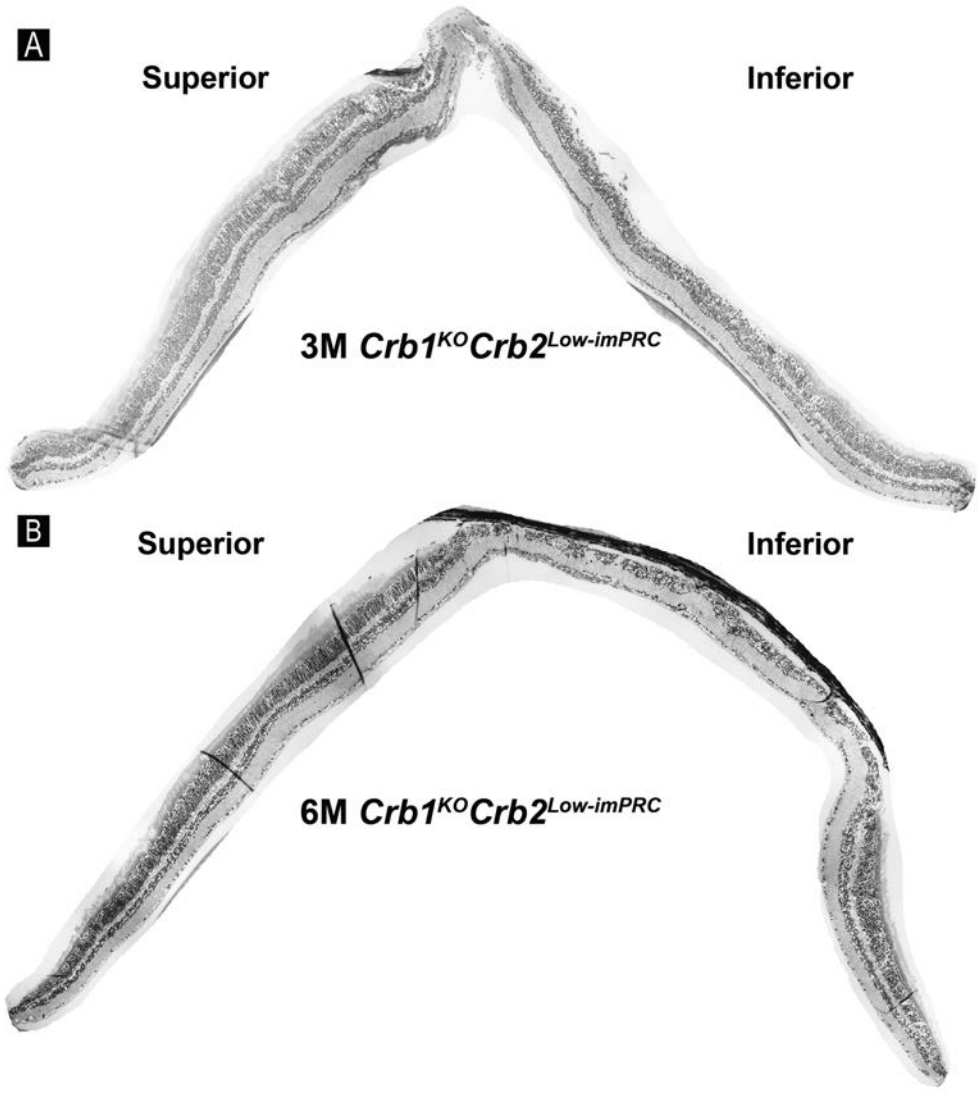

Supplemental Figure 4: Abnormal layering and superior/inferior asymmetry in aged *Crb1^{KO}Crb2$^{Low-imPRC}$* mice. Toluidine-stained light microscopy (A, B). Toluidine-stained light microscopy (A, B). Retinal stitch of 3M and 6M *Crb1^{KO}Crb2$^{\Delta imPRC}$* mouse retina showing superior- inferior asymmetry (A and B, respectively).

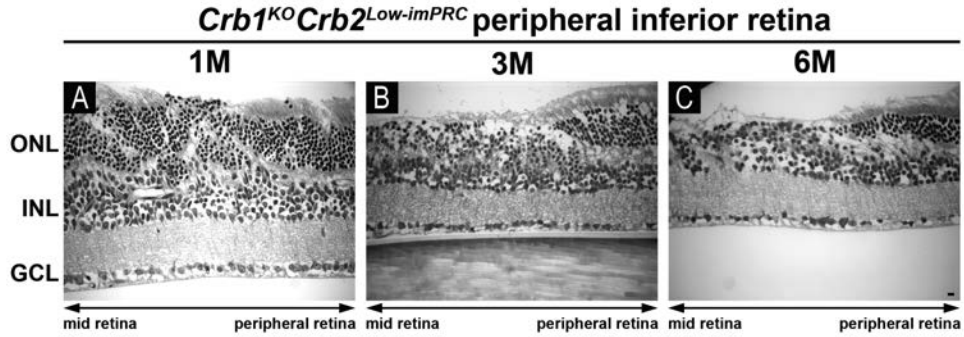

Supplemental Figure 5: Peripheral inferior retina phenotype transition in *Crb1*^{KO}*Crb2*$^{Low\text{-}imPRC}$ mice. Toluidine-stained light microscopy (A, B). Peripheral inferior retina phenotype transition in *Crb1*^{KO}*Crb2*$^{Low\text{-}imPRC}$ mice at 1-, 3-, and 6-months of age (A-C, respectively). GCL, ganglion cell layer; INL, inner nuclear layer; ONL, outer nuclear layer; ONH, optic nerve head. Scale bar: (A–C) 20 µm.

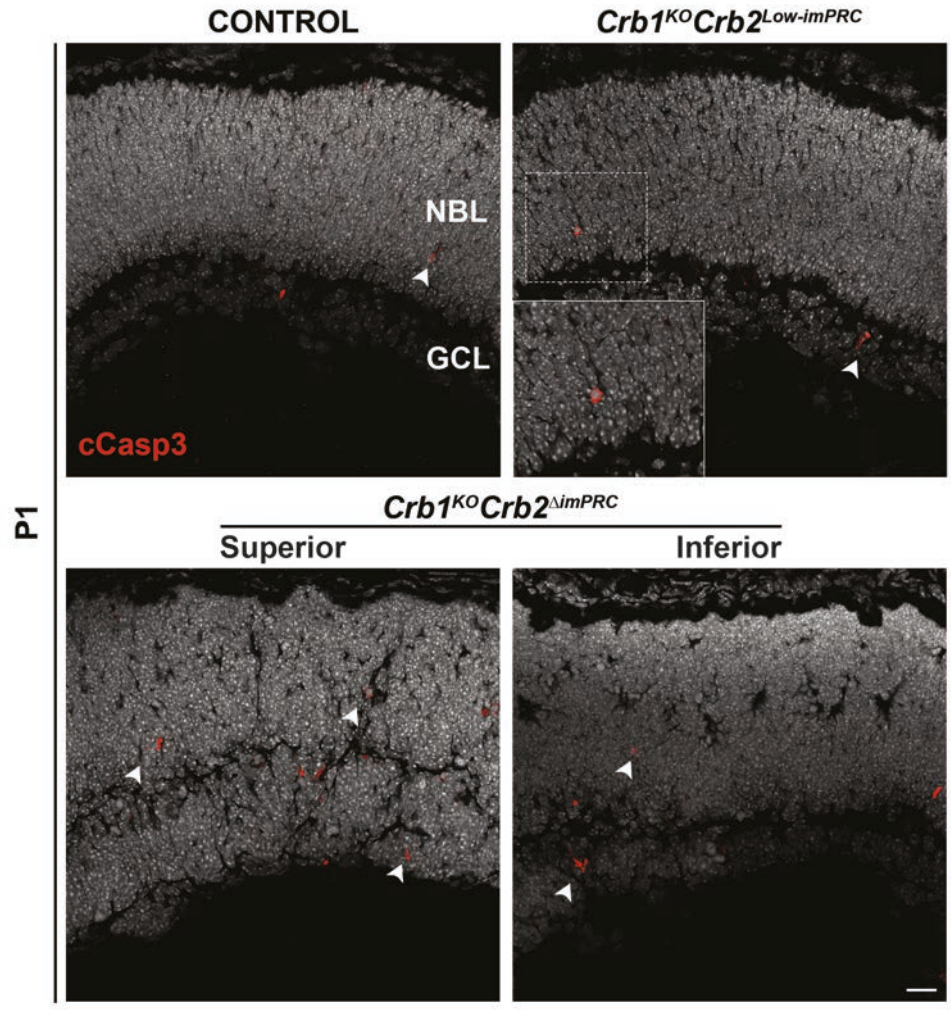

Supplemental Figure 6: Increase in cleaved Caspase-3 positive cells in early postnatal *Crb1^{KO}Crb2$^{\Delta imPRC}$* mice. Immunohistochemistry of cleaved Caspase-3 (cCasp3) positive apoptotic cells. Positive cells were found localised throughout the retina. Significantly more apoptotic cells were found in *Crb1^{KO}Crb2$^{\Delta imPRC}$* retina at P1 (Fig. 8I). GCL, ganglion cell layer; NBL, neuroblast layer. Scale bar: 20 µm.

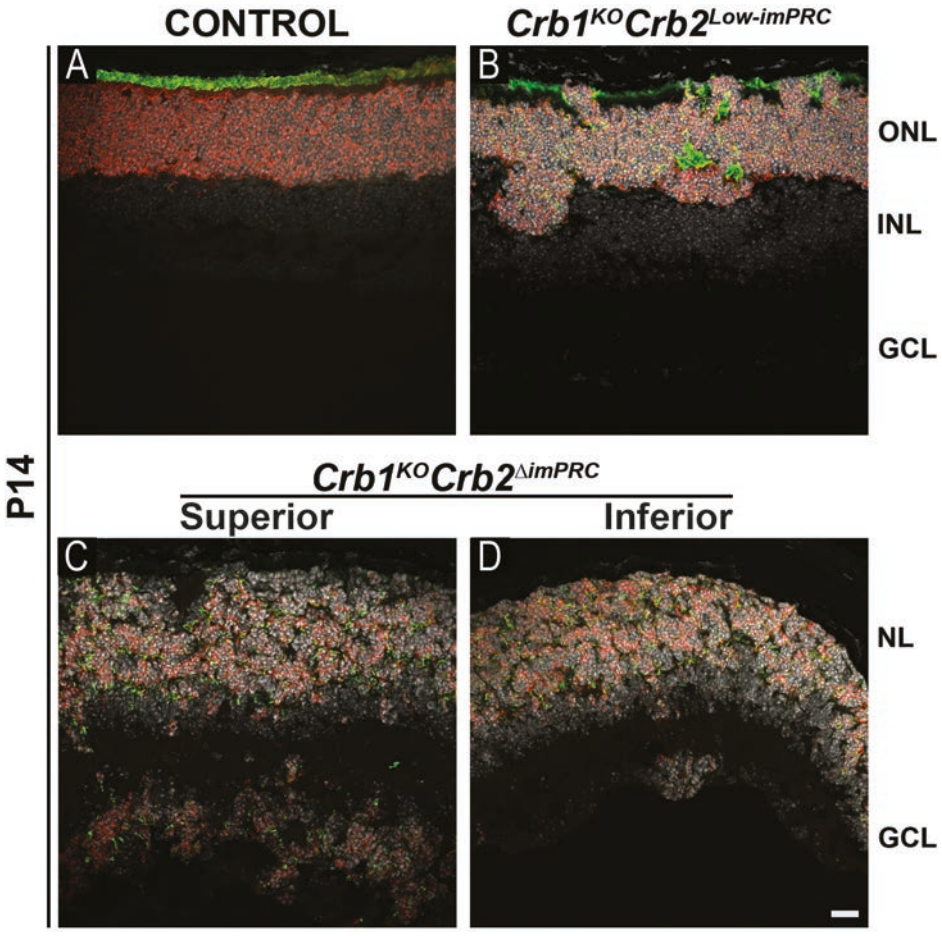

Supplemental Figure 7: Ectopic photoreceptors in ganglion cell layer of *Crb1^{KO}Crb2$^{\Delta imPRC}$* mice. Recoverin (Red) and rhodopsin (Green) positive photoreceptor cells localise to the ONL in control (A) and *Crb1^{KO}Crb2$^{Low\text{-}imPRC}$* (B) mice. Photoreceptors were found ectopically in the GCL in the superior (C) and inferior (D) retina of *Crb1^{KO}Crb2$^{\Delta imPRC}$* mice. GCL, ganglion cell layer; INL, inner nuclear layer; ONL, outer nuclear layer; NL, nuclear layer. Scale bar: 20 µm.

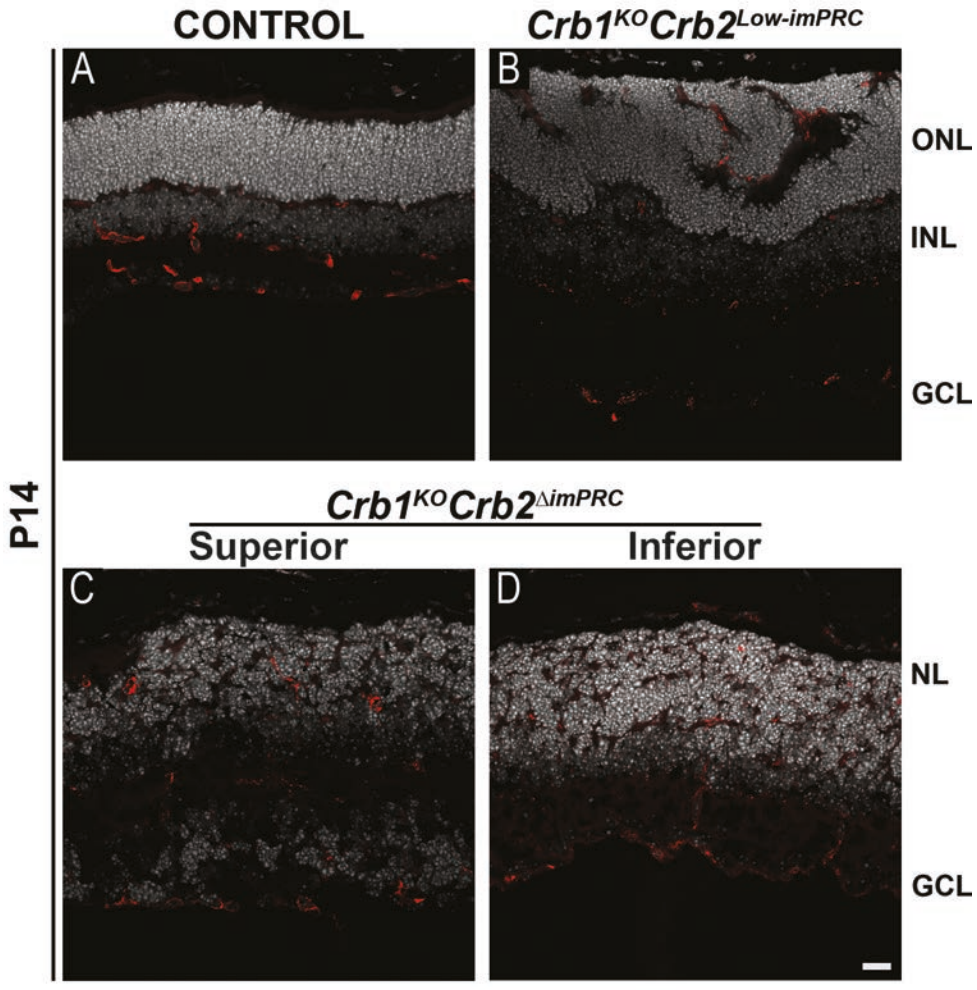

Supplemental Figure 8: Defects in retinal vasculature in *Crb1^{KO}Crb2$^{\Delta imPRC}$* and *Crb1^{KO}Crb2$^{Low\text{-}imPRC}$* mice. In control retina, Griffonia simplicifolia B4-isolectin (IB4, Red) stains for retinal vasculature and is restricted to the inner retina (A). In *Crb1^{KO}Crb2$^{Low\text{-}imPRC}$* mice, ectopic IB4 staining is found in rosettes of the ONL (B). In the Superior (C) and Inferior (D), *Crb1^{KO}Crb2$^{\Delta imPRC}$* retina IB4 is found mislocalised to the NL. GCL, ganglion cell layer; INL, inner nuclear layer; ONL, outer nuclear layer; NL, nuclear layer. Scale bar: 20 µm.